

Large volume behaviour of Yang-Mills propagators

Christian S. Fischer,^a Axel Maas,^{b,c} Jan M. Pawłowski,^d
and Lorenz von Smekal,^e

^a*Institut für Kernphysik, University of Technology, Schlossgartenstraße 9,
D-64289 Darmstadt, Germany*

^b*Instituto de Física de São Carlos, University of São Paulo, C. P. 369,
13560-970 São Carlos, SP, Brazil*

^c*Gesellschaft für Schwerionenforschung mbH, Planckstraße 1,
D-64291 Darmstadt, Germany*

^d*Institut für Theoretische Physik, University of Heidelberg, Philosophenweg 16,
D-62910 Heidelberg, Germany*

^e*Centre for the Subatomic Structure of Matter, School of Chemistry and Physics,
The University of Adelaide, SA 5005, Australia*

Abstract

We investigate finite volume effects in the propagators of Landau gauge Yang-Mills theory using Dyson-Schwinger equations on a 4-dimensional torus. In particular, we demonstrate explicitly how the solutions for the gluon and the ghost propagator tend towards their respective infinite volume forms in the corresponding limit. This solves an important open problem of previous studies where the infinite volume limit led to an apparent mismatch, especially of the infrared behaviour, between torus extrapolations and the existing infinite volume solutions obtained in 4-dimensional Euclidean space-time. However, the correct infinite volume limit is approached rather slowly. The typical scales necessary to see the onset of the leading infrared behaviour emerging already imply volumes of at least 10 to 15 fm in lengths. To reliably extract the infrared exponents of the infinite volume solutions requires even much larger ones. While the volumes in the Monte-Carlo simulations available at present are far too small to facilitate that, we obtain a good qualitative agreement of our torus solutions with recent lattice data in comparable volumes.

Key words: Yang-Mills theory, Propagators, Landau gauge, Finite volume effects
PACS: 12.38.Lg, 12.38.Aw, 14.70.Dj

1 Introduction

The infrared behaviour of the QCD Green's functions is known to contain essential information about the realisation of confinement in the covariant continuum formulation of QCD in terms of local field systems [1]. To extract this information from studies of correlation functions in a finite volume it is most important to address the volume dependence of the long-range, *i.e.* infrared, behaviour of these correlations. It is only when this dependence is under control that firm conclusions can be drawn from infinite volume extrapolations.

In this paper we revisit the elementary 2-point correlation functions, *i.e.* the propagators, of pure Yang-Mills theory without quarks in a finite volume. Using covariant gauges, and here in particular the Landau gauge, these are the gluon and the ghost propagators. These are perhaps the most important examples of how Green's functions relate to confinement in this formulation. Their infrared behaviour is sensitive to confinement according to the scenarios of Kugo and Ojima [2,3], and of Gribov and Zwanziger [4,5]. In Landau gauge these scenarios predict an infrared vanishing gluon propagator and an infrared enhanced ghost propagator (the latter was pointed out in [6]; for a review, see [1]).

Qualitatively, finite-volume effects are expected to distort the infrared properties of 2-point correlation functions for momenta approaching $2\pi/L$, where L is the finite length of the system in the corresponding direction. For pure Yang-Mills theory the momentum scale for confinement is set by Λ_{QCD} , which is of the order of 200 – 400 MeV, somewhat dependent on the scheme.¹ This implies that for lengths around $L_c = 2\pi/\Lambda_{\text{QCD}}$, of the order 3 – 6 fm, the finite volume will already have a considerable effect on the infrared behaviour of these confinement-sensitive correlations. Eventually, of course, when further decreasing the volume down to the sub-Fermi regime, confinement will be lost altogether.

In present Monte-Carlo simulations, using lattice Landau gauge, the gluon and ghost propagators of pure $SU(2)$ and $SU(3)$ gauge theory in four dimensions are obtained in volumes of the order of L_c in length, in some cases even somewhat larger than L_c [8,9,10,11]. However, despite clear indications in favour of the qualitative infrared behaviour of both the gluon and the ghost propagator, as predicted by continuum studies, some quantitative discrepancies still remain. In particular, apart from some indications from the volume scaling of the zero momentum gluon propagator, a systematic and statistically significant verification of its infrared suppression from lattice data in 4 dimensions is still lacking.²

As far as the continuum studies are concerned, on the other hand, we are nowadays in the quite comfortable situation that a variety of different non-perturbative approaches all lead to the same infrared behaviour for the propagators in the infinite volume limit. These include studies of their Dyson-Schwinger Equations (DSEs) [14], of the Fokker-Planck type diffusion equa-

¹ *E.g.*, $\Lambda_{\overline{MS}} \approx 240$ MeV for $N_f = 0$ from the lattice determination by the ALPHA Collaboration [7].

² This is different in Coulomb gauge and interpolating gauges, where a stronger suppression is expected from the Gribov-Zwanziger scenario, and where this infrared suppression of the gluon propagator *is* observed on the lattice already in rather small volumes [12,13].

tions of Stochastic Quantisation [15], and of the Functional Renormalisation Group Equations (FRGEs) [16].

In order to understand the origin of the remaining discrepancies observed between the functional methods in the continuum and the lattice Landau gauge simulations, it is an obvious and necessary step forward to adapt the continuum methods to finite volumes. The techniques to solve Dyson-Schwinger equations on a finite four dimensional torus with periodic boundary conditions have recently been developed and applied to the various propagator DSEs of Landau gauge QCD [17,18,19]. The infinite volume limit, however, remained unclear in these studies. Here we specifically address this question and explicitly demonstrate how the infrared behaviour known from the previous studies of functional methods is approached in the infinite volume limit also by the DSE solutions on a finite torus.

In fact, this is to be expected. The perturbative and the confining regime are separated by a cross-over, the scale of which is Λ_{QCD} , the dynamical scale. As pointed out in previous infrared studies [14,16,20], for the investigation of the infrared regime of the correlation functions we have to consider Λ_{QCD} an ultraviolet scale which is large compared to all external momenta p involved, *i.e.*, $p \ll \Lambda_{\text{QCD}}$. As mentioned above, for the emergence of continuum infrared physics we need in addition that $2\pi/L \ll p$. To reliably extract infrared critical exponents from finite volume studies we therefore need a clear separation of scales with a sufficient number of different momentum values all in the range

$$\frac{2\pi}{L} \ll p \ll \Lambda_{\text{QCD}} . \quad (1.1)$$

Indeed, the same scale separation was used in the infrared analysis of the functional RGEs [16,20], where an explicit infrared momentum cut-off k is introduced and plays a role analogous to that by the finite volume. In the functional RG infrared-studies it is precisely this regime, $k \ll p \ll \Lambda_{\text{QCD}}$, that is required to lead to the same infrared behaviour as in the other functional continuum investigations without such infrared cut-off [14,15]. In the available studies of the DSEs on a symmetric hypertorus, on the other hand, this same limit has not been explicitly obtained as yet. In the present work we fill this gap by presenting a refined infrared analysis.

Because of the necessary separation of scales (1.1), the actual lattice sizes L necessary to achieve this separation for a sufficiently wide range of momentum values need to be much larger than L_c . From our numerical analysis we estimate that this might well require lengths L of the order of 40 fm, so that reliable lattice determinations of the infrared exponents of the gluon and ghost propagators on reasonably fine lattices are likely to remain unfeasible for some time to come. Corresponding $SU(2)$ simulations on rather large lattices in three dimensions [21] confirm this by showing a slow but steady convergence towards the three dimensional infinite volume limit, as predicted by DSE studies [15,22].

Meanwhile, we explicitly demonstrate this convergence here for the DSE solutions in a finite 4-dimensional volume by investigating the behaviour of the propagators on length scales in the range given by (1.1). Sec. 2 is devoted to analytic results. After a brief summary of the infrared

behaviour of the propagators from infinite volume studies in Sec. 2.1, we discuss the torus DSEs and their proper renormalisation in Sec. 2.2. The question of zero modes is addressed in Sec. 2.3. The infrared behaviour of the torus-DSE solutions and the volume dependence of the low-momentum modes are studied in Sec. 2.4. Our numerical results are presented in Sec. 3. This contains a brief description of the general procedure and the implementation of the renormalisation procedure in Secs. 3.1 and 3.2, and a detailed discussion of the numerical solutions for the gluon and ghost propagators in various volumes in Sec. 3.3. In Sec. 3.4 we present fits and extrapolations to model the approach towards the infinite volume limit, and in Sec. 3.5 we compare our solutions to the results of lattice simulations with similar volumes.

Our conclusions are provided in Sec. 4. We summarise that the presently available lattice data is consistent with the continuum results, if the consequences of finite-volume effects are properly taken into account. Moreover, the infinite-volume extrapolations of our torus-DSE solutions indicate that volumes of lengths of the order of 40 fm might be necessary to explicitly verify the infrared behaviour of the gluon and ghost propagators in the various functional continuum approaches, and to obtain reliable estimates from lattice simulations of the critical exponents indicative of this conformal infrared behaviour of the pure gauge theory in the infinite volume, the 4-dimensional Euclidean space-time.

2 Analytic Results

2.1 Dyson-Schwinger equations at infinite volume

The Dyson-Schwinger equations of QCD in 4-dimensional Euclidean space-time have been used very successfully to determine the Green's functions in particular of the Landau gauge [1,23].

For the propagators of the pure gauge theory in the Landau gauge the full momentum dependence is parametrised by two dimensionless dressing functions Z and G as follows,

$$D_{\mu\nu}^{ab}(p) = \delta^{ab} \left(\delta_{\mu\nu} - \frac{p_\mu p_\nu}{p^2} \right) \frac{Z(p)}{p^2},$$

$$D^{ab}(p^2) = -\delta^{ab} \frac{G(p)}{p^2},$$

where $D_{\mu\nu}^{ab}$ is the gluon propagator and D^{ab} is the propagator of the Faddeev-Popov ghosts.

The infrared behaviour of these dressing functions Z and G for gluons and ghosts is determined by one unique infrared exponent $0 < \kappa < 1$ [24,25],

$$Z_{\text{IR}}(p^2) \sim (p^2)^{2\kappa}, \quad G_{\text{IR}}(p^2) \sim (p^2)^{-\kappa}. \quad (2.2)$$

The exact value of this exponent κ depends only on the infrared behaviour of a single invariant function $A(k^2; p^2, q^2)$ [14] which multiplies the tree-level structure in the full ghost-gluon vertex. Here k^2 denotes the gluon momentum and p^2 and q^2 are the (anti)ghost momenta. In ghost/anti-ghost symmetric gauges, such as the Landau gauge, A is symmetric under the exchange of the ghost momenta, $A(k^2; q^2, p^2) = A(k^2; p^2, q^2)$. If this function is furthermore assumed to be finite and regular in the origin at $k^2 = p^2 = q^2 = 0$, then the value of the infrared exponent κ is [14]

$$\kappa = \kappa_c = \frac{93 - \sqrt{1201}}{98} \approx 0.595. \quad (2.3)$$

This regularity assumption is all that is needed to obtain this otherwise exact result. The same value of κ was obtained independently at the same time using a bare vertex (which is trivially regular) from the time-independent (equilibrium version of the) diffusion equation of Stochastic Quantisation [15]. In the corresponding truncation of the functional RGEs a range of values roughly between 0.54 and κ_c is possible with (2.3) representing the special value obtained for an optimised flow [16,20].

The same regularity assumption implicitly underlies all these studies and produces the unique result (2.3). Other values for κ in the range $1/2 \leq \kappa < 1$ are possible, if the tree-level structure A of the ghost-gluon vertex has infrared divergences associated with any of its legs [14].

So how justified is this regularity assumption? It is relatively easy to see that $A(p^2; 0, p^2) = A(p^2; p^2, 0) = 1$ in Landau gauge. An independent and different argument, from the non-renormalisation of the ghost-gluon vertex in Landau gauge [26], perturbatively at all orders, implies $A(p^2; p^2, p^2) = 1$ in a symmetric momentum subtraction scheme. If this argument remains true beyond perturbation theory it fixes the infrared limit of A along a second direction. Lattice simulations of the ghost-gluon vertex have so far tested the line $A(0; p^2, p^2)$ in $SU(2)$ and $SU(3)$ for momenta p down to values of the order of Λ_{QCD} , and obtained results consistent with $A(0; p^2, p^2) = 1$ with no systematic indications of any momentum dependence along this third direction either [27,28,29].³ While none of this can prove the infrared regularity of this ghost-gluon vertex structure, there is certainly no evidence to the contrary at present.

Probably more importantly, however, there is a self-consistent scheme to solve the full hierarchy of DSEs in the pure gauge theory asymptotically in the infrared [31]. Remember that the complete system of DSEs forms an infinite set of coupled non-linear integral equations between all n -point Green's functions. The self-consistent infrared-asymptotic solution to the whole tower of n -point Green's functions obtained in [31] reflects the infrared fixed-point behaviour of the pure gauge theory. The ghost-gluon vertex *is* regular in the infrared in this solution, which incorporates (2.2) and leads to a simple counting scheme for generalised power laws of this kind for all n -point Green's functions. Moreover, it has recently been proven that this solution is unique among this class of parametrisations of a conformal infrared behaviour [32].

Because of the non-renormalisation of the ghost-gluon vertex in Landau gauge, the ghost and

³ For more results in $SU(2)$, including some different kinematic regimes, see [30].

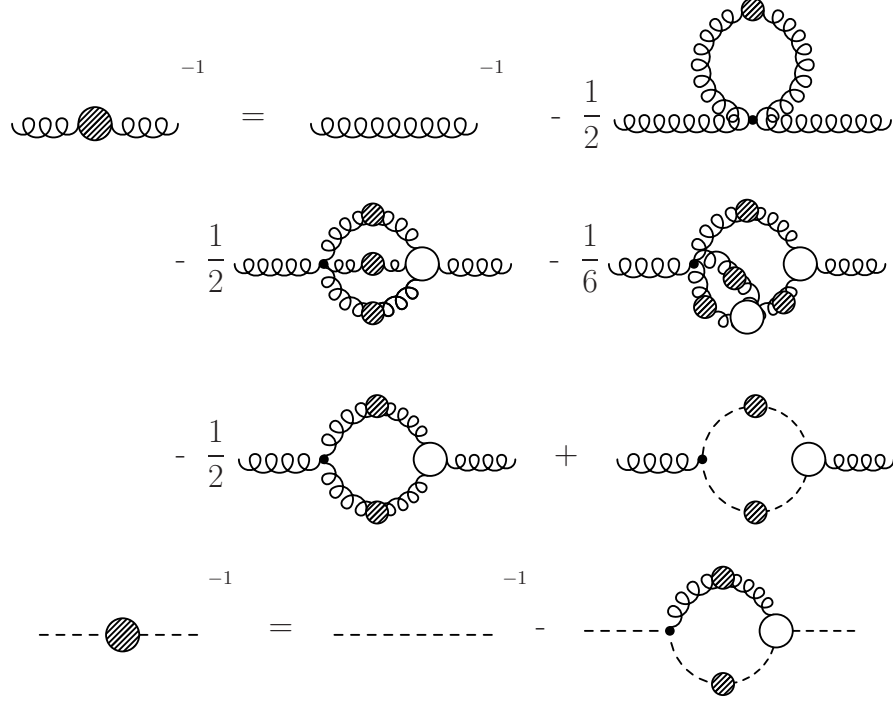


Fig. 1. The propagator DSEs. Curly lines are gluons and dotted lines are ghosts. Lines with a large filled dot represent full propagators. Vertices with a small dot are bare and with a large dot are full and constructed in this truncation.

gluon dressing functions provide a non-perturbative definition of the running coupling in this gauge via the RG invariant product [25]

$$\alpha(p^2) = \alpha(\mu^2) G(p^2)^2 Z(p^2), \quad (2.4)$$

where μ^2 is the renormalisation point. It approaches a finite positive value for $p^2 \rightarrow 0$ in four dimensions for all $0 < \kappa < 1$. The value of this infrared fixed-point depends on κ , *i.e.*, on the infrared properties of the ghost-gluon vertex (it vanishes at both end points of this interval, for $\kappa \rightarrow 0$ and for $\kappa \rightarrow 1$). Moreover, the maximal value of the coupling at the infrared fixed-point is that obtained for the infrared-regular ghost-gluon vertex, with $\kappa = \kappa_c$ from (2.3), which yields [14],

$$\alpha(0) = \alpha_c = \frac{8\pi}{N_c} \frac{\Gamma^2(\kappa_c - 1) \Gamma(4 - 2\kappa_c)}{\Gamma^2(-\kappa_c) \Gamma(2\kappa_c - 1)} \approx \frac{4\pi}{N_c} 0.709 \approx 8.9/N_c, \quad (2.5)$$

for N_c colours. This implies $\alpha_c \approx 4.46$ for $SU(2)$ and $\alpha_c \approx 2.97$ for $SU(3)$.

Numerical solutions of the DSEs can only be obtained in specific truncation schemes. For the coupled system of ghost and gluon propagator DSEs, given diagrammatically in Fig. 1, one such scheme has been defined in [17,34]. It uses a bare ghost-gluon vertex, a choice well justified by both lattice studies [27,28,29,30] as well as calculations using the vertex DSE [33]. Furthermore

an Ansatz for the three-gluon vertex has been used that ensures the correct infrared and ultraviolet limits of the solutions for the ghost and gluon propagators. Contributions involving the four-gluon interaction have been neglected, a choice which only affects the intermediate momentum regime [1,23]. The resulting numerical solutions of the ghost-gluon system have been reported in [34] and are included here again in Sec. 3. In the following we will denote these solutions as 'infinite volume solutions' as opposed to the 'torus solutions' discussed in the next sections. Note that for the latter we assume the continuum limit in a finite volume even though, strictly speaking, our numerical solutions in Sec. 3 are obtained on a discrete and finite set of momentum values. The continuum limit thereby corresponds to removing the ultraviolet cut-off, of course. In Sec. 3.3 we will verify that the residual cut-off dependences of the propagators are negligible. Unlike lattice simulations, where disentangling discretisation errors and finite volume effects can be a rather challenging task, it is therefore not necessary to study the continuum limit more carefully for the DSE solutions, provided a consistent renormalisation scheme is implemented.

2.2 Dyson-Schwinger equations on a torus

For the formulation of the Dyson-Schwinger equations of Fig. 1 in a 4-dimensional hypercubic volume L^4 of length L in all directions, with periodic boundary conditions, the momentum integrals in the infinite volume DSEs are replaced by sums,

$$\int \frac{d^4 q}{(2\pi)^4} (\dots) \longrightarrow \frac{1}{L^4} \sum_{n \in \mathbb{Z}^4} (\dots), \quad (2.6)$$

where the four dimensional vector of integers $n \in \mathbb{Z}^4$ labels the discrete momentum values $q_n = (2\pi/L) n$. In the following we truncate the DSEs shown in Fig. 1 such that the diagrams with (bare) four-gluon vertices are neglected, analogous to the truncation scheme used in the infinite volume computations as mentioned above. Denoting the gluon and ghost dressing functions by Z_L and G_L in the finite volume, their corresponding DSEs become,

$$\begin{aligned} \frac{1}{Z_L(k)} = Z_3 - \frac{g^2 N_c \tilde{Z}_1}{3} \frac{1}{L^4} \sum_n \frac{q_n \mathcal{P}(k) p_n G_L(q_n) G_L(p_n)}{k^2 q_n^2 p_n^2} \\ + \frac{g^2 N_c Z_1}{3} \frac{1}{L^4} \sum_n \frac{H_{3g}(p_n, q_n, k) N(p_n, q_n, k) Z_L(q_n) Z_L(p_n)}{k^2 q_n^2 p_n^2}, \end{aligned} \quad (2.7)$$

$$\frac{1}{G_L(k)} = \tilde{Z}_3 - g^2 N_c \tilde{Z}_1 \frac{1}{L^4} \sum_n \frac{k \mathcal{P}(p_n) q_n G_L(q_n) Z_L(p_n)}{k^2 q_n^2 p_n^2}, \quad (2.8)$$

with $p_n = k - q_n$. We furthermore use the translational invariance of the sums under $q_n \rightarrow q_n + 2\pi m/L$ with $m \in \mathbb{Z}^4$. The abbreviation $k \mathcal{P}(p) q$ denotes a contraction with the transverse momentum tensor, *i.e.* $k \mathcal{P}(p) q = k_\mu P_{\mu\nu}(p) q_\nu$ with $P_{\mu\nu}(p) = \delta_{\mu\nu} - p_\mu p_\nu / p^2$. The integration kernel

$N(p, q, k)$ and the Ansatz for the dressing function $H_{3g}(p, q, k)$ of the three-gluon vertex can be found in Refs. [17,18]. Note also that the above equations are not restricted to external momenta $k_n = (2\pi/L)n$, and k may or may not be one of these discrete values. For $k \neq (2\pi/L)n$, the Equations (2.7), (2.8) should be symmetrised in q_n and p_n .

The renormalisation is done in the infinite volume limit, which suffices for finiteness, analogously to finite temperature field theory. This can be shown on the level of the functional DSEs by adding and subtracting the infinite volume DSEs and identifying the renormalisation constants $Z_i \in \{Z_1, \tilde{Z}_1, Z_3, \tilde{Z}_3\}$ at infinite volume with those in a finite volume $Z_{i,L}$,

$$Z_{i,L} = Z_i. \quad (2.9)$$

Such a scheme facilitates the approach towards infinite volume. We emphasise that the scheme does not imply the same RG conditions at finite and infinite volume. Applying the renormalisation scheme (2.9) to the propagator DSEs (2.8) and (2.7), and furthermore using the result $\tilde{Z}_1 = 1$ in Landau gauge [26], we obtain

$$\begin{aligned} \frac{1}{Z_L(k)} = \frac{1}{Z(k'^2)} - \frac{g^2 N_c}{3} & \left(\frac{1}{L^4} \sum_n \frac{q_n \mathcal{P}(k) p_n G_L(q_n) G_L(p_n)}{k^2 q_n^2 p_n^2} - \int \frac{d^4 q}{(2\pi)^4} \frac{q \mathcal{P}(k') p' G(q) G(p')}{k'^2 q^2 p'^2} \right) \\ & + \frac{g^2 N_c Z_1}{3} \left(\frac{1}{L^4} \sum_n \frac{H_{3g}(p_n, q_n, k) N(p_n, q_n, k) Z_L(q_n) Z_L(p_n)}{k^2 q_n^2 p_n^2} \right. \\ & \quad \left. - \int \frac{d^4 q}{(2\pi)^4} \frac{H_{3g}(p', q, k') N(p', q, k') Z(q) Z(p')}{k'^2 q^2 p'^2} \right), \quad (2.10) \end{aligned}$$

$$\begin{aligned} \frac{1}{G_L(k)} = \frac{1}{G(k'^2)} - g^2 N_c & \left(\frac{1}{L^4} \sum_n \frac{k \mathcal{P}(p_n) q_n G_L(q_n) Z_L(p_n)}{k^2 q_n^2 p_n^2} \right. \\ & \quad \left. - \int \frac{d^4 q}{(2\pi)^4} \frac{k' \mathcal{P}(p') q G(q) Z(p')}{k'^2 q^2 p'^2} \right). \quad (2.11) \end{aligned}$$

The sum of the renormalisation terms in each of the two equations is, of course, momentum independent. The dependence on k' (with $p' = k' - q$) is thus an illusion. Any momentum value can be used equally. A particular and convenient choice below will be $k' = k$ (and $p' = p$).

The RG-scheme in (2.10),(2.11) facilitates our discussion of finite volume effects in the next section. The subtraction is $O(4)$ -symmetric and hence keeps the $O(4)$ -symmetry violations by the finite volume at a minimum. Moreover, this subtraction scheme is not restricted to the ghost and gluon propagators. It can be extended self-consistently to the DSEs of general Green's functions and general truncation schemes [20]. The implementation of this scheme in our numerical treatment of the propagator DSEs is discussed in Sec. 3.2.

2.3 Zero modes

An important subtlety concerns the ghost propagator and vertex functions. In the covariant gauges there are constant ghost zero modes which decouple completely from the theory. This is a consequence of the unfixed global gauge symmetry. The action does not depend on these constant ghost/anti-ghost modes, as it only couples to derivatives of the ghost and anti-ghost fields. As a consequence, the Faddeev-Popov operator can only be inverted for non-vanishing momenta $p \neq 0$. The ghost propagator is thus only defined with the corresponding projection such that $G_L(q)$ has the property that

$$G_L(q_n) = G_L(q_n)(1 - \delta_{n0}) . \quad (2.12)$$

Eq. (2.12) entails that the zero ghost-momentum terms are absent in the propagator DSEs. Note that in contrast the gluon zero modes do contribute to the loop sums as the gluonic vertex functions do depend on the constant gauge field. However, transversality is not well-defined at vanishing gluon momentum. Hence, we have to separate the zero-momentum contribution explicitly, writing,

$$D_{L\mu\nu}(p_n) = \delta_{\mu\nu} L^2 C_L \delta_{n0} + P_{\mu\nu}(p_n) \frac{Z_L(p_n)}{p_n^2} (1 - \delta_{n0}) . \quad (2.13)$$

Here C_L is some dimensionless constant which represents the value of the gluon propagator at momentum zero in units of L^2 . In principle, this constant is to be determined self-consistently from the set of algebraic equations representing the propagator DSEs for the discrete momenta in the periodic L^4 box along with the remaining $Z(p_n)$. Up to the factor 4/3 from the tensor structure, the value of the gluon propagator at momentum zero in the finite volume is expected to be of approximately the same magnitude as for the lowest non-zero modes p_n . This is what is typically observed in lattice simulations also. For the parametrisation (2.13) it implies that

$$C_L \sim \frac{Z_L(2\pi/L)}{(2\pi)^2} . \quad (2.14)$$

Eqs. (2.12) and (2.13) are important to obtain well-defined algebraic equations from the DSEs. These equations are closed among themselves only when the external momentum coincides with one of the discrete momenta $k = k_m = (2\pi/L) m$ for $m \in \mathbb{Z}^4$. With Eqs. (2.12) and (2.13) we rewrite the gluon DSE (2.7) for $Z(k_m)$ with $m \neq n$ and $p_{mn} = k_m - q_n$, and separately for C_L with $m = 0$, as

$$\begin{aligned} \frac{1}{Z_L(k_m)} &= Z_3 + \frac{g^2 N_c}{3 L^4} \sum_{n \neq 0, m} \frac{k_m^2 q_n^2 - (k_m q_n)^2}{k_m^4 q_n^2 p_{mn}^2} G_L(q_n) G_L(p_{mn}) + \dots \\ &= Z_3 + \frac{g^2 N_c}{3} \frac{1}{(2\pi)^4} \sum_{n \neq 0, m} \frac{m^2 n^2 - (mn)^2}{m^4 n^2 (m - n)^2} G_L(q_n) G_L(p_{mn}) + \dots , \quad m \neq 0 , \end{aligned} \quad (2.15)$$

$$C_L^{-1} = \frac{g^2 N_c}{4} \frac{1}{L^2} \sum_{n \neq 0} \frac{1}{q_n^2} G_L^2(q_n) + \dots = \frac{g^2 N_c}{4} \frac{1}{(2\pi)^2} \sum_{n \neq 0} \frac{G_L^2(q_n)}{n^2} + \dots \quad (2.16)$$

We did not repeat the contributions from the 3-gluon loop explicitly here again. Note that in the gauge-invariantly regularised full theory gauge invariance implies that the DSE (2.16) for C_L must be ultraviolet finite, and of the order given by (2.14). Hence there is no counter-term in the equation for C_L . The term from the ghost loop alone, which is given explicitly here, is not finite, of course. Nonetheless, its apparent ultraviolet divergence, which has to be cancelled by those of the terms not given explicitly here, does not affect the infrared analysis, as will be shown below.

With the separation (2.13), the ghost DSE (2.8) for $m \neq 0$ becomes,

$$\frac{1}{G_L(k_m)} = \tilde{Z}_3 - \frac{g^2 N_c}{L^4} \sum_{n \neq 0, m} \frac{k_m^2 q_n^2 - (k_m q_n)^2}{k_m^2 q_n^4 p_{mn}^4} G_L(q_n) Z_L(p_n) - \frac{g^2 N_c C_L}{L^2 k_m^2} G_L(k_m) \quad (2.17)$$

There is no DSE for $m = 0$ in this case. In the momentum range (1.1) of interest here, we have $(2\pi)^2 \ll L^2 k_m^2$. With dressing functions $G(k_m)$, $Z(k_m)$ of the order one, and C_L of the order of magnitude given by (2.14), the gluonic zero mode contribution to the ghost DSE (2.17) is therefore suppressed by an explicit factor of $(2\pi)^2/(L^2 k_m^2)$ as compared to the other terms in this momentum range.

An important practical consequence of the above analysis is that we can safely drop the contributions of the gluonic zero mode in the DSEs. This is important for our numerical analysis, *c.f.*, Sec. 3.

2.4 Infrared analysis

We proceed with an infrared analysis following that of [14,16]. Due to the missing $O(4)$ -symmetry the dressing functions $Z_L(k)$ and $G_L(k)$ are functions of the individual components k_i , and not of k^2 alone. When using an $O(4)$ -symmetric ultraviolet cut-off in (2.7),(2.8), however, we have approximate $O(4)$ symmetry for momenta $k^2 L^2 \geq 1$. Therefore, in order to simplify the analysis, we may neglect the residual $O(4)$ -symmetry violation considering an $O(4)$ -average with respect to the external momentum k in the propagator DSEs.

For $k \rightarrow 0$, with $k \neq k_m = (2\pi/L) m$, the gluon equation (2.15) only depends on $G_L(q_n)$ and $G_L(p_n) \rightarrow G_L(q_n)$ (where $p_n = k - q_n$, *c.f.*, Sec. 2.2, and thus $p_n \rightarrow q_n$) with $q_n^2 \geq 4\pi/L^2$. Note that this momentum regime is below the lowest momentum obtainable in the numerical calculations in Sec. 3.

The ghost dressing functions in the ghost loop of (2.15) therefore remain finite in this limit (for monotonically decreasing $G_L(q_n)$ the upper bound will be $G_L(2\pi/L)$). Hence, we deduce from the right hand side of the gluon equation that $Z(k)/k^2$ has a finite yet direction-dependent

limit for $k \rightarrow 0$. The angle dependence in this limit relates to the missing $O(4)$ -symmetry on the torus. After angular averaging we thus write

$$Z_L(k^2) \equiv \int \frac{d\omega_k}{2\pi^2} Z_L(k) \propto \frac{k^2}{\mu_Z^2(L)} \left(1 + \mathcal{O}(k^2/\mu_Z^2)\right), \quad (2.18)$$

for $k \rightarrow 0$. Eq. (2.18) displays the behaviour of a dressing function of a particle with a screening mass $\mu_Z(L)$. Inserting this behaviour into the ghost equation (2.17) we analogously deduce for the ghost dressing function that

$$G_L(k^2) \equiv \int \frac{d\omega_k}{2\pi^2} G_L(k) \propto 1 + \mathcal{O}(k^2/\mu_G^2), \quad (2.19)$$

for $k \rightarrow 0$. In contrast to the gluon propagator, the ghost propagator remains massless in the finite volume. Due to the ghost screening mass $\mu_G(L)$ the ghost dressing function $G_L(k)$ is infrared finite at finite L , however. The infinite-volume renormalisation scheme of Eqs. (2.9), (2.10) and (2.11) will guarantee that both screening masses $\mu_{Z/G}(L) \rightarrow 0$ in the infinite volume limit $L \rightarrow \infty$.

By construction, the averaged dressing functions only depend on the magnitude of momentum. We emphasise that this approximation does not change powers in k^2 . In particular, it will not affect the infrared exponents of momenta $k \gg 2\pi/L$. In the regime (1.1) we can expand the dressing functions $Z_L(k^2)$ and $G_L(k^2)$ about their leading physical infrared behaviour,

$$\begin{aligned} Z_L(k^2) &= Z_{\text{IR}} \left(\frac{\Lambda_{\text{QCD}}^2}{k^2 + \mu_Z^2} \right)^{\kappa_{Z_L}} \frac{k^2}{k^2 + \mu_Z^2} \left(1 + \delta Z \left(\frac{k^2}{\Lambda_{\text{QCD}}^2}, \frac{1}{k^2 L^2} \right) \right), \\ G_L(k^2) &= G_{\text{IR}} \left(\frac{\Lambda_{\text{QCD}}^2}{k^2 + \mu_G^2} \right)^{\kappa_{G_L}} \left(1 + \delta G \left(\frac{k^2}{\Lambda_{\text{QCD}}^2}, \frac{1}{k^2 L^2} \right) \right), \end{aligned} \quad (2.20)$$

with

$$\delta Z(0,0) = \delta G(0,0) = 0, \quad (2.21)$$

and possibly k -dependent κ_{Z_L/G_L} but constant $Z_{\text{IR}}, G_{\text{IR}}$. For $k \rightarrow 0$ we arrive at the limits (2.18) and (2.19) with subleading powers depending on $k^2/\mu_{Z/G}^2$. The finite volume corrections are suppressed with $1/(k^2 L^2)$, and the confinement scale works as an UV cut-off leading to corrections of the order $k^2/\Lambda_{\text{QCD}}^2$. The corresponding terms are hidden in the corrections δZ and δG respectively. We could also have absorbed the screening 'masses' $\mu_{Z/G}$ into the definitions of the $\delta Z/\delta G$ -corrections, but we prefer to keep them explicitly in this infrared Ansatz for later convenience.

For $\Lambda_{\text{QCD}}^2 \gg k^2 \gg \mu_{G/Z}^2$ we are left with the physical infrared behaviour, $Z_L(k^2) \sim (k^2)^{-\kappa_{Z_L}}$,

$G_L(k^2) \sim (k^2)^{-\kappa_{G_L}}$. In particular, for $L \rightarrow \infty$ the parametrisations (2.20) tend towards the infinite volume infrared forms,

$$\begin{aligned} Z_L(k^2) &\rightarrow Z(k^2) = Z_{\text{IR}} \left(\frac{\Lambda_{\text{QCD}}^2}{k^2} \right)^{-2\kappa} \left(1 + \delta Z \left(\frac{k^2}{\Lambda_{\text{QCD}}^2}, 0 \right) \right), \\ G_L(k^2) &\rightarrow G(k^2) = G_{\text{IR}} \left(\frac{\Lambda_{\text{QCD}}^2}{k^2} \right)^{\kappa} \left(1 + \delta G \left(\frac{k^2}{\Lambda_{\text{QCD}}^2}, 0 \right) \right), \end{aligned} \quad (2.22)$$

with the limits

$$\kappa_{Z_L} \rightarrow -2\kappa, \quad \kappa_{G_L} \rightarrow \kappa, \quad \text{and} \quad \mu_{Z/G} \rightarrow 0 \quad \text{for} \quad L \rightarrow \infty. \quad (2.23)$$

This follows immediately from the renormalised DSEs (2.10), (2.11).

We are also quantitatively interested in the approach towards the infinite volume solutions, and concentrate on momenta

$$\frac{k^2}{\Lambda_{\text{QCD}}^2} \rightarrow 0, \quad (2.24)$$

which is achieved formally by taking the limit $\Lambda_{\text{QCD}}^2 \rightarrow \infty$. The limit of asymptotically large volumes, on the other hand, is obtained from $k^2 \rightarrow \infty$. In general, the infinite-volume DSEs will require renormalisation also for $\Lambda_{\text{QCD}}^2 \rightarrow \infty$. This is different from the standard perturbative UV-renormalisation in that contributions of momenta at about Λ_{QCD} are removed. Once the infinite volume DSEs are properly renormalised, however, the limit $k^2 \rightarrow \infty$ can be performed without further subtractions in the torus DSEs (2.7) and (2.8): when the right hand sides in the form of (2.10) and (2.11) are used, the results remain finite.

We first insert the parametrisations (2.20) into the gluon Dyson-Schwinger equation (2.10). After angular averaging, we consider the leading contribution from the ghost loop in the momentum regime (1.1) which becomes

$$\begin{aligned} \frac{1}{Z_{\text{IR}}} \left(\frac{\Lambda_{\text{QCD}}^2}{k^2 + \mu_Z^2} \right)^{-\kappa_{Z_L}} \frac{k^2 + \mu_Z^2}{k^2} &= \frac{g^2 N_c}{3} \frac{G_{\text{IR}}^2}{L^4} \times \\ &\sum_{n \neq 0, n_k} \frac{q_n \mathcal{P}(k) q_n}{k^2 q_n^2 p_n^2} \left(\frac{\Lambda_{\text{QCD}}^2}{q_n^2 + \mu_G^2} \right)^{\kappa_{G_L}} \left(\frac{\Lambda_{\text{QCD}}^2}{p_n^2 + \mu_G^2} \right)^{\kappa_{G_L}} + \dots \end{aligned} \quad (2.25)$$

Herein, n_k labels the loop momentum closest to k , *i.e.*, the minimum of p_n^2 . For momenta in the range (1.1) the corrections due to δZ , δG can be neglected. Moreover, because the ghost loop dominates in this momentum regime, we can safely drop all the other contributions, not given explicitly here. The infinite volume renormalisation vanishes due to the value of $\kappa_c > 0.5$

in (2.3): the momentum integral in (2.10) is finite and agrees with $1/Z(k'^2)$. We immediately conclude that

$$\lim_{q^2 \rightarrow \infty} \kappa_{G_L}(q^2) > 0.5, \quad (2.26)$$

to guarantee finiteness of (2.25). In the approximate expression (2.25), $\Lambda_{\text{QCD}}^2/k^2$ and $k^2/\mu_{Z/G}^2$ are all assumed to be sufficiently large but still finite. When these ratios tend to infinity we recover one of the infinite volume DSE conditions for the critical exponent κ_c (2.3) and the infrared fixed point α_c (2.5) in [14].

Note also that the momentum sums in (2.25) receive their main contribution for momenta at about k^2 . Upon rearranging (2.25) we obtain up to sub-leading terms,

$$\frac{4\pi}{\alpha_c N_c} = \left(\frac{\Lambda_{\text{QCD}}^2}{k^2 + \mu_Z^2} \right)^{\kappa_{Z_L} + 2\kappa_{G_L}} I_{Z_L}(\kappa_{G_L}, k, \frac{2\pi}{L}), \quad (2.27)$$

where

$$I_{Z_L}(\kappa, k, \frac{2\pi}{L}) = \frac{16\pi^2}{3L^4} \sum_{n \neq 0, n_k} \frac{1}{p_n^2 q_n^2} \frac{q_n \mathcal{P}(k) q_n}{k^2 + \mu_Z^2} \left(\frac{k^2 + \mu_Z^2}{q_n^2 + \mu_G^2} \right)^\kappa \left(\frac{k^2 + \mu_Z^2}{p_n^2 + \mu_G^2} \right)^\kappa, \quad (2.28)$$

and $\alpha_c = (g^2/4\pi) Z_{\text{IR}} G_{\text{IR}}^2$. Recall that Eq. (2.27) holds for $\mu_{Z/G}^2 \ll k^2 \ll \Lambda_{\text{QCD}}^2$. For its left hand side to have a non-vanishing and finite value in the limit (2.24) with $\Lambda_{\text{QCD}}^2 \rightarrow \infty$, we need to have at sufficiently large but still finite L , as in the infinite volume limit,

$$\kappa_{Z_L} + 2\kappa_{G_L} = 0. \quad \text{Thus we define analogously, } \kappa_{G_L} \equiv \kappa_L, \quad \kappa_{Z_L} \equiv -2\kappa_L, \quad (2.29)$$

as in the $L \rightarrow \infty$ limit. Then, the dependence on the scale Λ_{QCD} is eliminated from the infrared analysis as necessary. We obtain,

$$\frac{4\pi}{\alpha_c N_c} = I_{Z_L}(\kappa_L, k, \frac{2\pi}{L}), \quad (2.30)$$

and it is easy to verify that in the second limit, that of large volume via $k^2 \rightarrow \infty$, this explicitly leads to the infrared condition (2.5) for α_c from the infinite-volume gluon DSE in [14], as

$$\begin{aligned} I_{Z_L}(\kappa_L, k, \frac{2\pi}{L}) &\rightarrow I_Z(\kappa_L) = 16\pi^2 \int \frac{d^4 q}{(2\pi)^4} \frac{1}{q^2 p^2} \frac{q \mathcal{P}(k) q}{3k^2} \left(\frac{k^2}{q^2} \right)^{\kappa_L} \left(\frac{k^2}{p^2} \right)^{\kappa_L} \\ &= \frac{1}{2} \frac{\Gamma^2(-\kappa_L) \Gamma(2\kappa_L - 1)}{\Gamma^2(\kappa_L - 1) \Gamma(4 - 2\kappa_L)}, \end{aligned} \quad (2.31)$$

for $k^2 \rightarrow \infty$. The condition in Eq. (2.30) therefore implies that $\kappa_L \rightarrow \kappa_c$ in this limit, as expected.

The infrared dominant contribution for $\Lambda_{\text{QCD}}^2 \rightarrow \infty$ in the ghost DSE still needs ultraviolet renormalisation, as it does in the infinite volume case. With (2.20), (2.22) we obtain the corresponding contributions to the renormalised ghost DSE (2.11), with $k' = k$,

$$\begin{aligned} \frac{1}{G_{\text{IR}}} \left(\frac{\Lambda_{\text{QCD}}^2}{k^2 + \mu_G^2} \right)^{-\kappa_L} &= \frac{1}{G_{\text{IR}}} \left(\frac{\Lambda_{\text{QCD}}^2}{k^2} \right)^{-\kappa_c} - g^2 N_c G_{\text{IR}} Z_{\text{IR}} \left(\frac{1}{L^4} \sum_{n \neq 0, n_k} \frac{k \mathcal{P}(p_n) k}{k^2 q_n^2 (p_n^2 + \mu_Z^2)} \times \right. \\ &\quad \left. \left(\frac{\Lambda_{\text{QCD}}^2}{q_n^2 + \mu_G^2} \right)^{\kappa_L} \left(\frac{\Lambda_{\text{QCD}}^2}{p_n^2 + \mu_Z^2} \right)^{-2\kappa_L} - \int \frac{d^4 q}{(2\pi)^4} \frac{k \mathcal{P}(p) k}{k^2 q^2 p^2} \left(\frac{\Lambda_{\text{QCD}}^2}{q^2} \right)^{\kappa_c} \left(\frac{\Lambda_{\text{QCD}}^2}{p^2} \right)^{-2\kappa_c} \right). \end{aligned} \quad (2.32)$$

This equation is ultraviolet finite because the (weakly) momentum dependent exponent $\kappa_L \rightarrow \kappa_c$, whenever the momentum argument of the corresponding dressing function becomes large (of the order of Λ_{QCD}), as already derived from the ghost loop in the gluon DSE above. Eq. (2.32) can be rewritten in the form,

$$\frac{4\pi}{\alpha N_c} = I_{G_L}(\kappa_L, k, \frac{2\pi}{L}) - \left(\frac{k^2}{k^2 + \mu_G^2} \right)^{\kappa_L} \left(\frac{\Lambda_{\text{QCD}}^2}{k^2} \right)^{\kappa_L - \kappa_c} [I_G(\kappa_c, k, 0) - I_G(\kappa_c)] . \quad (2.33)$$

Here, $I_G(\kappa, k, 2\pi/L)$ is the corresponding loop sum (as explicitly given in (2.39) below), which is ultraviolet divergent in this case. This divergence is cancelled by the likewise ultraviolet divergent infinite volume integral expression

$$I_G(\kappa, k, 0) = -16\pi^2 \int \frac{d^4 q}{(2\pi)^4} \left(\frac{1}{q^2} \right)^2 \left(\frac{q^2}{k^2} \right)^{1-\kappa} \left(\frac{k^2}{p^2} \right)^{1-2\kappa} \frac{k_\mu \mathcal{P}_{\mu\nu}(p) k_\nu}{k^2} , \quad (2.34)$$

whose finite contributions are independent of k and given by [14]

$$I_G(\kappa) = -\frac{3}{2} \frac{\Gamma^2(-\kappa) \Gamma(2\kappa - 1)}{\Gamma(-2\kappa) \Gamma(\kappa - 1) \Gamma(\kappa + 3)} . \quad (2.35)$$

That leaves only the divergent part in the terms in brackets on the right of Eq. (2.33) to remove the ultraviolet divergence of the loop $I_G(\kappa_L, k, 2\pi/L)$ (with $\kappa_L \rightarrow \kappa_c$ at large momenta). Eq. (2.33) is the analogue to Eq. (2.30) from the gluon DSE.

Alternatively, we can use $k' = 0$ in the renormalisation terms of (2.11) to compute the infinite-volume ghost renormalisation constant \tilde{Z}_3 explicitly [14],

$$\tilde{Z}_3 = g^2 N_c \frac{3}{4} \int \frac{d^4 q}{(2\pi)^4} \frac{Z(q^2) G(q^2)}{q^4} . \quad (2.36)$$

Using the infinite volume infrared forms (2.22) for asymptotically large Λ_{QCD} with $O(4)$ -symmetric ultraviolet cut-off Λ_{UV} this becomes

$$\tilde{Z}_3 \rightarrow \tilde{Z}_3^{\text{IR}} = g^2 N_c \frac{3}{4} \frac{Z_{\text{IR}} G_{\text{IR}}}{16\pi^2} \left(\frac{\Lambda_{\text{UV}}^2}{\Lambda_{\text{QCD}}^2} \right)^\kappa. \quad (2.37)$$

Of course, asymptotically large Λ_{QCD} in this case means $\Lambda_{\text{QCD}} \rightarrow \Lambda_{\text{UV}}$, and Λ_{QCD} acts as the ultraviolet momentum cut-off in the infrared analysis as explained above. Then, with (2.20) in the ghost DSE (2.8), we obtain from the leading infrared contribution in this limit

$$\frac{4\pi}{\alpha_c N_c} = I_{G_L}(\kappa_L, k, \frac{2\pi}{L}) + \frac{3}{4} \left(\frac{\Lambda_{\text{QCD}}^2}{k^2 + \mu_G^2} \right)^{\kappa_L}. \quad (2.38)$$

The loop sum herein is cut off at $q_n^2 \leq \Lambda_{\text{QCD}}^2 \equiv (2\pi/L)^2 N_\Lambda^2$,

$$I_{G_L}(\kappa_L, k, \frac{2\pi}{L}) = -\frac{16\pi^2}{L^4} \sum_{n \neq 0, n_k}^{n^2 \leq N_\Lambda^2} \frac{k \mathcal{P}(p_n) k}{k^2 q_n^2 (p_n^2 + \mu_Z^2)} \left(\frac{k^2 + \mu_G^2}{q_n^2 + \mu_G^2} \right)^{\kappa_L} \left(\frac{p_n^2 + \mu_Z^2}{k^2 + \mu_Z^2} \right)^{2\kappa_L} \quad (2.39)$$

where for asymptotically large q_n^2 , approaching Λ_{QCD}^2 , the sum over the loop-momentum q_n tends to the corresponding integral because of the large number $L^4 q_n^2 dq_n^2 / (16\pi^2)$ of modes in $[q_n^2, q_n^2 + dq_n^2]$. The ultraviolet divergence of the loop with cut-off Λ_{QCD} is therefore subtracted correctly by the infinite volume counter-term in (2.38), which thus remains finite in the $\Lambda_{\text{QCD}}^2 \rightarrow \infty$ limit as required.

As for the ghost-loop contribution to the gluon DSE, *c.f.*, Eq. (2.30) with (2.31), in the second limit of large $L^2 k^2$ we recover the infrared self-consistency condition from the infinite-volume ghost DSE of [14]. Using Eqs. (2.30) and (2.38), or (2.33), we furthermore obtain the leading corrections $\propto 1/(k^2 L^2)$ as follows:

First, expanding $I_{Z_L}(\kappa_L, k, 2\pi/L)$ in Eq. (2.28) for large k^2 , from the ghost loop of the gluon DSE (2.30), we obtain

$$\frac{4\pi}{\alpha_c N_c} = I_Z(\kappa_L) \left\{ 1 + (2\kappa_L - 1) \frac{\mu_Z^2}{k^2} - 2\kappa_L \frac{(2\kappa_L - 1)(3 - 2\kappa_L)}{(1 + \kappa_L)(1 - \kappa_L)} \frac{\mu_G^2}{k^2} \right\} + \mathcal{O}\left(\frac{1}{L^4 k^4}\right). \quad (2.40)$$

Analogously, from the ghost DSE, condition (2.38) becomes

$$\begin{aligned} \frac{4\pi}{\alpha_c N_c} = I_G(\kappa_L) \left\{ 1 - \left(\kappa_L - \frac{\kappa_L^2 (2 + \kappa_L)}{(1 + \kappa_L)(1 - \kappa_L)} \right) \frac{\mu_G^2}{k^2} \right. \\ \left. - \frac{(2\kappa_L - 1)(2 + \kappa_L)}{4(1 - \kappa_L)} \frac{\mu_Z^2}{k^2} \right\} + \mathcal{O}\left(\frac{1}{L^4 k^4}\right). \end{aligned} \quad (2.41)$$

The leading order herein again reproduces the corresponding infinite volume condition which entails $\kappa_L \rightarrow \kappa_c$ in the limit $k^2 \rightarrow \infty$, as

$$\frac{4\pi}{\alpha_c N_c} = I_Z(\kappa_c) = I_G(\kappa_c) . \quad (2.42)$$

With $I_Z(\kappa)$, $I_G(\kappa)$ from Eqs. (2.31), (2.35) it follows that $\kappa_c = (93 - \sqrt{1201})/98 = 0.59535\dots$ and $\alpha_c = 2.9717\dots$ (for $N_c = 3$), see [14].

Secondly, for the leading corrections to this limit, we furthermore let

$$\kappa_L \equiv \kappa_L(L^2 k^2) = \kappa_c - \frac{c_\kappa}{L^2 k^2} + \mathcal{O}\left(\frac{1}{L^4 k^4}\right) . \quad (2.43)$$

In addition, parametrising the leading L -dependence of the screening masses via

$$\mu_Z^2 = \frac{c_Z}{L^2} , \quad \text{and} \quad \mu_G^2 = \frac{c_G}{L^2} , \quad (2.44)$$

we obtain from the leading corrections in (2.40) and (2.41), respectively,

$$\begin{aligned} c_\kappa \frac{I'_Z(\kappa_c)}{I_Z(\kappa_c)} &= (2\kappa_c - 1) c_Z - \frac{\kappa_c(2 + \kappa_c)}{6(1 - \kappa_c)} c_G , \\ c_\kappa \frac{I'_G(\kappa_c)}{I_G(\kappa_c)} &= -\frac{(2\kappa_c - 1)(2 + \kappa_c)}{4(1 - \kappa_c)} c_Z - \left(\kappa_c - \frac{\kappa_c^2(2 + \kappa_c)}{(1 + \kappa_c)(1 - \kappa_c)} \right) c_G . \end{aligned} \quad (2.45)$$

The fact that we have 3 unknowns, c_κ , c_Z and c_G , from only 2 equations here reflects an ambiguity in our parametrisations (2.20) of the finite-volume infrared behaviour of the gluon and ghost dressing functions in the momentum regime of (1.1). As a parametrisation of the leading corrections to the infinite-volume infrared forms with originally 2 parameters in each of the dressing functions, $Z_L(k^2)$ and $G_L(k^2)$, Eqs. (2.20) are somewhat redundant, of course. Even after eliminating one of the originally 2 exponents, the residual redundancy is manifest here. An $L^2 k^2$ independent exponent is excluded, however, as $c_\kappa = 0$ implies that also $c_Z = c_G = 0$ for $\kappa_c = (93 - \sqrt{1201})/98$.

In fact, in units of c_κ , Eqs. (2.45) yield numerical values

$$c_Z \approx 238 c_\kappa , \quad c_G \approx 86 c_\kappa . \quad (2.46)$$

Because $c_\kappa > 0$ for positive $c_{Z/G}$ (*c.f.*, Eqs. (2.44)), with the definition of c_κ in (2.43), we find that κ_L approaches κ_c from below.

Moreover, Eqs. (2.46) imply that the momentum dependence of the exponent $\kappa_L(L^2 k^2)$ is a rather weak effect in comparison to the influence of the screening masses, which thus account

for the dominant finite-volume corrections at sufficiently large $k^2 L^2$. Therefore, a quantitatively good approximation for large volumes and momenta in (1.1) is given by

$$\begin{aligned} Z_L(k^2) &= Z_{\text{IR}} \left(\frac{\Lambda_{\text{QCD}}^2}{k^2 + \mu_Z^2} \right)^{-2\kappa_c} \frac{k^2}{k^2 + \mu_Z^2}, \\ G_L(k^2) &= G_{\text{IR}} \left(\frac{\Lambda_{\text{QCD}}^2}{k^2 + \mu_G^2} \right)^{\kappa_c}, \end{aligned} \quad (2.47)$$

with the infinite volume κ 's. With this approximation of neglecting the momentum dependence of the infrared exponent κ_L , estimates of the screening masses $\mu_{Z/G}$ can in principle be obtained from Eqs. (2.30) and (2.33), (or (2.38)) at $k^2 = 0$ rather than considering large k^2 for the leading $1/(L^2 k^2)$ corrections as done so far. Because the resulting equations will then necessarily involve the summations over the discrete loop momenta, such an estimate would already need a numerical solution to these equations. Here, we rather present our full numerical solutions to the torus DSEs in the next section. The masses extracted from these full solutions in Sec. 3.4 are in good agreement with the ratio c_Z/c_G determined here.

Finally, inserting the screening masses $\mu_{Z/G} = c_{Z/G}/L^2$ with L -independent coefficients $c_{Z/G}$ into the IR-asymptotics (2.47), for vanishing momentum k^2 with $\delta Z = \delta G = 0$ and $-\kappa_{Z_L}/2 = \kappa_{G_L} \approx \kappa_c$ in (2.20), we obtain an estimated behaviour with L of the infrared limit of the gluon and ghost dressing functions as

$$\lim_{k^2 \rightarrow 0} \frac{Z_L(k^2)}{k^2} \propto L^{2(1-2\kappa_c)}, \quad (2.48)$$

$$\lim_{k^2 \rightarrow 0} G_L(0) \propto L^{2\kappa_c}. \quad (2.49)$$

The L -dependence of the dressing functions at $k = 0$ mimics the infrared leading momentum behaviour. In particular, as $(1 - 2\kappa_c) \approx -0.19$, this implies that the zero momentum gluon propagator is expected to decrease extremely slowly with the volume $V = L^4$ towards zero in the infinite volume limit $\propto V^{-\epsilon}$ with an exponent $\epsilon = (2\kappa_c - 1)/2$ which is smaller than 0.1. The infrared limit of the ghost propagator, on the other hand, increases faster than linear with the length L . We will compare these qualitative features to the full numerical solution in the next section.

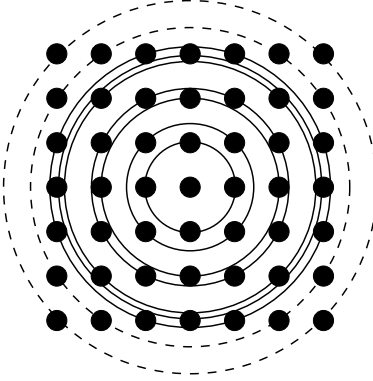


Fig. 2. Sketch of the momentum grid dual to the four-torus. The summation over complete hyperspheres is indicated by fully drawn circles. The hyperspheres depicted by dashed lines are not complete if one uses Cartesian cutoffs instead of an $O(4)$ invariant one.

3 Numerical results

3.1 The momentum lattice

As already mentioned in the previous section, in a 4-dimensional hypercubic volume $V = L^4$ with periodic boundary conditions, the momentum integrals of the infinite volume DSEs are replaced by sums, *c.f.*, (2.6). For the numerical treatment of the equations it is convenient to rearrange these summations in a spherical coordinate system [17]. A two-dimensional illustration of this procedure is given in Fig. 2. We thus write (2.6) in the form

$$\frac{1}{L^4} \sum_{n \in \mathbb{Z}^4} (\dots) = \frac{1}{L^4} \sum_{m,j} (\dots), \quad (3.50)$$

where m labels sums over hyperspheres, each containing all momentum vectors of the same absolute value and j numbers the individual vectors on a given hypersphere. The resulting double sum corresponds to the splitting between radial and angular integrals in the infinite volume DSEs. This correspondence is very good for large hyperspheres (*i.e.*, in the ultraviolet momentum region), where a large number of vectors on a given sphere samples the angular dependence of the integral kernels well. However, in the infrared, *i.e.*, on the innermost spheres, this sampling will be poor, thus resulting in hypercubic artefacts. We will identify these in our solutions in Sec. 3.3. Note, however, that the sole dependence of the dressing functions on the squared momenta is not touched by these artefacts. We explicitly verified that the dressing functions $Z(p^2)$ and $G(p^2)$ do not depend on the direction of the momentum p .

For numerical reasons we also have to introduce a momentum cut-off that limits the extend of the momentum lattice. In the infinite volume formulation such a cut-off Λ_{UV} is $O(4)$ -invariant. The resulting renormalised dressing functions are independent of the value of Λ_{UV} , as they

should be in a renormalisable quantum field theory. In general, this is no longer true on a four-torus and we expect cut-off artefacts. It turns out that these effects are sizeable only when $O(4)$ -symmetry is badly broken as is the case, *e.g.*, when restricting the sums in (2.6) in each Cartesian direction. Much better results are obtained, if an (approximately) $O(4)$ -invariant cut-off is introduced by using the summation procedure (3.50) and summing only over such hyperspheres which do not receive any further vectors when enlarging the momentum grid. In Fig. 2 these are indicated by the solid lines as opposed to the dashed ones. Since these fully occupied outer spheres typically contain a large number of momentum vectors, the corresponding 'angular sum' over j is close in value to the corresponding angular integrals in the infinite volume limit and is thus a good approximate representation of the corresponding $O(4)$ -symmetry. Note that we have used a similar procedure in our infrared analysis around and below Eq. (2.37).

3.2 Renormalisation procedure

Further details of our numerical method to solve the coupled system of Eqs. (2.8), (2.7) have been described in [17,18,35] and shall not be repeated here. The only major difference to previous calculations of DSEs on the torus is a modification of the renormalisation conditions. These modifications turn out to have a substantial impact on the large volume limit.

The propagator DSEs (2.10) and (2.11) resulting from the renormalisation condition (2.9) in Sec. 2 make the approach towards the infinite volume solutions at large torus volumina transparent. A direct numerical implementation of eqs. (2.10) and (2.11) requires a sufficiently large UV-cut-off Λ_{UV} . Unfortunately, for reasons of CPU-time we are restricted to a rather low UV-cut-off of the order of $\Lambda_{UV} = 2 - 3$ GeV. For such a low cutoff one encounters convergence problems in the infinite volume DSEs which prevent a reliable extraction of the ghost and gluon renormalisation factors \tilde{Z}_3 and Z_3 . We therefore adjust the renormalisation procedure of Sec. 2 to the numerics as explained in the following.

We substitute the infinite volume subtractions in eqs. (2.10) and (2.11) by subtractions on the torus at a fixed scale s^2 , which in general does not have to be equal to the renormalisation point. In the symbolical notation

$$\frac{1}{G(p^2)} = \tilde{Z}_3 + g^2 N_c \Pi_{ghost}(p^2), \quad (3.51)$$

$$\frac{1}{Z(p^2)} = Z_3 + g^2 N_c \Pi_{glue}(p^2), \quad (3.52)$$

for the equations (2.7) and (2.8) this procedure yields

$$\frac{1}{G(p^2)} = \frac{1}{G(s^2)} + g^2 N_c \left(\Pi_{ghost}(p^2) - \Pi_{ghost}(s^2) \right), \quad (3.53)$$

$$\frac{1}{Z(p^2)} = \frac{1}{Z(s^2)} + g^2 N_c \left(\Pi_{glue}(p^2) - \Pi_{ghost}(s^2) \right), \quad (3.54)$$

similarly to (2.10) and (2.11). The renormalisation constants Z_3 and \tilde{Z}_3 are traded for two input values at $G(s^2)$ and $Z(s^2)$. These values are not independent of each other. In the infinite volume limit this can be seen from the Slavnov-Taylor identity

$$\tilde{Z}_1(\mu^2, \Lambda_{UV}^2) = Z_g(\mu^2, \Lambda_{UV}^2) \tilde{Z}_3(\mu^2, \Lambda_{UV}^2) Z_3^{1/2}(\mu^2, \Lambda_{UV}^2), \quad (3.55)$$

In Landau gauge, the ghost-gluon vertex is ultraviolet finite, and therefore one always has the choice of setting $\tilde{Z}_1 = 1$ [26]. Thus for a fixed Z_g , corresponding to a fixed choice of the renormalised coupling $\alpha(\mu^2) = g^2(\mu^2)/4\pi$, one has a unique relation between the renormalisation factors \tilde{Z}_3 and Z_3 of the ghost and gluon propagators. In terms of renormalisation conditions this corresponds to the relation

$$G(\mu^2)^2 Z(\mu^2) = 1, \quad (3.56)$$

i.e. the ghost and gluon dressing functions may not be renormalised independently for a given renormalised coupling [25]. Accordingly, the input values $G(s^2)$ and $Z(s^2)$ have to be chosen to satisfy (3.56). In the infrared analysis in Sec. 2 these could be taken from the well-known infinite volume infrared solutions in accordance with the renormalisation conditions (2.9). For a numerical solution, however, this is not an option.

The simplest way to implement (3.56) would be to choose $s^2 = \mu^2$, fix $Z(s^2)$ and $G(s^2) = 1/Z(s^2)^{1/2}$. Unfortunately this is not possible: the function $g \rightarrow \mu^2$ is not known before the equations are solved completely and accordingly choosing a specific g is not sufficient to determine the value of μ^2 . One thus chooses an arbitrary, usually large, subtraction point s^2 , fixes $Z(s^2)$ and then solves for a range of values for $G(s^2)$. In the infinite volume limit one obtains continuous and differentiable solutions only for an extremely narrow range of values $G(s^2)$ around the correct one implementing (3.56) [34].

However, this is no longer true on the compact manifold. We found that for given values of $g(\mu^2)$ and $Z(s^2)$ one can generate a continuous array of solutions by varying $G(s^2)$. These solutions all behave different in the infinite volume limit. In previous works [17,18] these ambiguities have been resolved by reading off $Z(s^2)$ and $G(s^2)$ at a large s^2 from the infinite volume solution. However, this procedure is not sufficient. Since one works with a fixed cutoff Λ_{UV} on the torus, one encounters $O(1/\Lambda_{UV})$ effects in the ultraviolet momentum region, similar to $O(a)$ -effects in lattice QCD. Thus the ultraviolet behaviour of the torus solutions is slightly different from the infinite volume results. This difference is significant for the renormalisation procedure and in turn affects the infrared behaviour of the solutions and also the scaling behaviour with volume.

To avoid these UV-cutoff effects we modify the RG procedure by utilising the analytic results in Sec. 2: the RG condition on the torus is adjusted to approach the infinite volume RG condition in the limit of very large volumes as implemented in Sec. 2 in (2.10) and (2.11). To that end we

choose $G(s^2)$ for fixed g and $Z(s^2)$ accordingly. As a result we find that the values of $Z(s^2)$ and $G(s^2)$ are different but still close to the corresponding values of the infinite volume solution.

To summarise: we find that $O(a)$ -effects have to be accounted for in the renormalisation procedure for DSEs on the torus to obtain the correct infinite volume limit. This technical improvement compared to previous works [17,18] allows us in turn to reliably explore the large volume behaviour of the ghost and gluon propagators.

3.3 Propagators

Our numerical results for the ghost and gluon propagator on different volumes are shown in the two graphs of Figure 3. The momentum scale is fixed by comparison with corresponding lattice calculations: we demand that the maximum of the gluon dressing function in the DSE-approach occurs at the same momentum scale as in the lattice dressing function. Hereby we assume implicitly that truncation errors due to the neglect of the gluonic two-loop diagrams only mildly affect the position of the maximum. As a crosscheck we compare the resulting values of the DSE and the lattice gluon propagator at the lowest momentum point accessible on manifolds of similar volume. The result, shown explicitly in Sec. 3.5 below, suggests that scale uncertainties relative to the lattice scale might roughly be of the order of 10 percent.

We discuss results on seven different volumes $V = L^4$; the corresponding box lengths L are given in the legends of Figure 3. One clearly observes that the infinite volume solutions of the gluon propagator $D(p^2)$ and ghost dressing function $G(p^2)$ are more and more approached by the torus solutions with increasing volume. This tendency will be quantified in Sec. 3.4. Qualitatively one can see the following behaviour from the plot: the propagator seems to be divergent at volumes of $V \approx (4-8 \text{ fm})^4$. Note that these volumes are already large compared to the ones used in most lattice calculations of observables. For even larger volumes the propagator bends downwards to reach a plateau at roughly $V \approx (9 \text{ fm})^4$. For volumes larger than $V \approx (10 \text{ fm})^4$ the propagator is infrared vanishing and therefore qualitatively similar to the infinite volume limit given in (2.2) and (2.3).

This finding becomes even more pronounced when one applies momentum cuts: from the inlet of the graph for the gluon propagator one can see that the first three momentum points on the dual torus behave differently than the other points. In the language of Sec. 3.1 this means that the 'angular sum' over j on these spheres is by no means a good representation of the corresponding angular integrals in the infinite volume limit. If one omits these points in the representation of $D(p^2) = Z(p^2)/p^2$ and $G(p^2)$, then the turnover of the gluon propagator shifts from roughly $V \approx (9 \text{ fm})^4$ to $V \approx (11 \text{ fm})^4$. In such a representation only the propagator of our largest volume, $V = (13.8 \text{ fm})^4$, can be seen as infrared vanishing. Taken at face value this means that contemporary lattice calculations are still far away from the critical volume where the behaviour of the infinite volume solution can be deduced.

Similar conclusions can be drawn from the results for the ghost propagator. In Figure 3 we observe that the first two or three points on each result for the ghost bend away from the

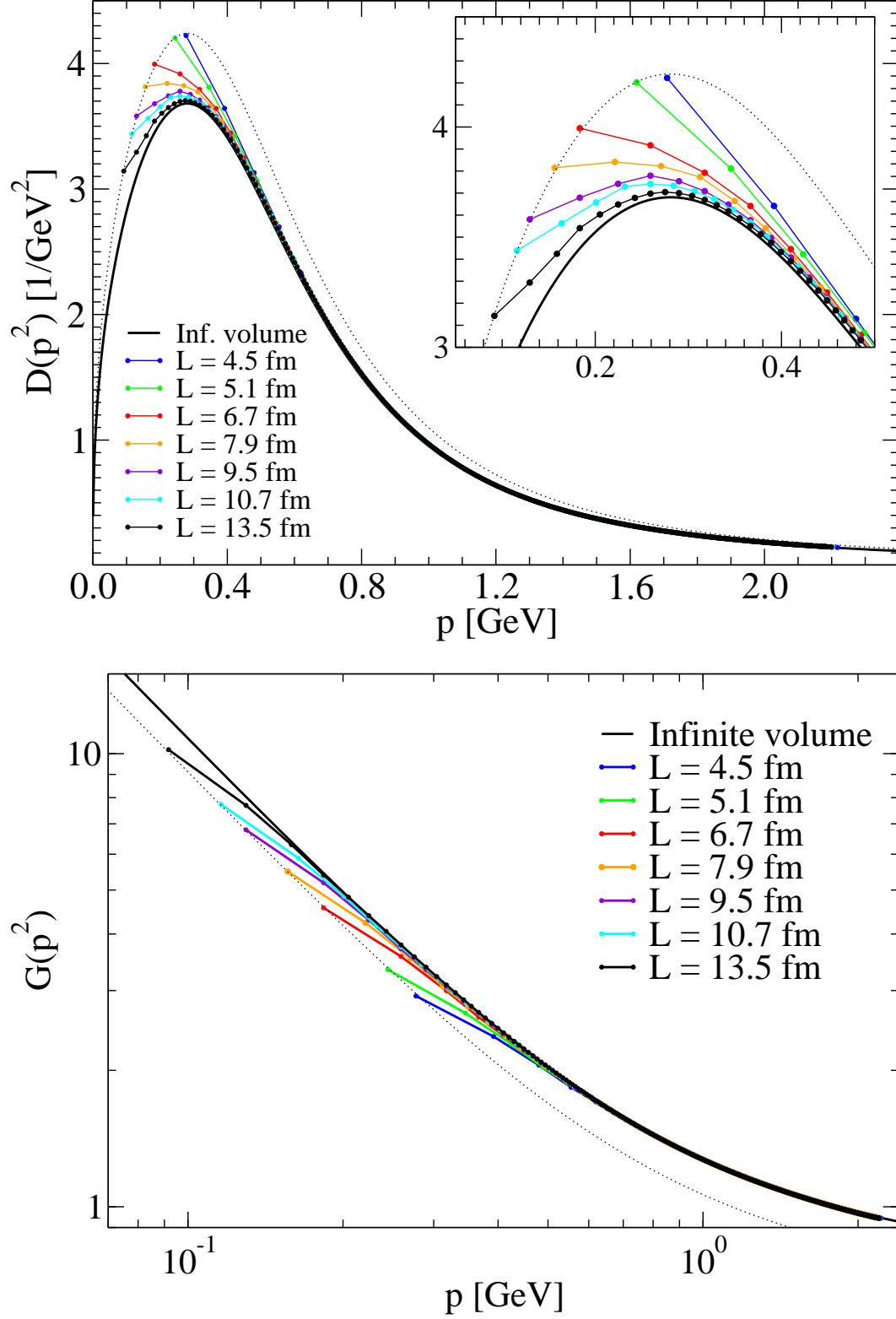


Fig. 3. Numerical solutions on tori with different volumes compared to the infinite volume limit. The upper graph shows the gluon propagator, whereas on the lower graph the ghost dressing function is depicted.

power law behaviour of the infinite volume solution. The remaining curves have more and more points on the 'scaling region' of the ghost dressing function, where the infinite volume power law develops. The critical volume, where the full infinite volume power law can be seen on the torus, is of roughly the same size as the one for the gluon propagator.

It is interesting to note that the lowest momentum point of the gluon and ghost solutions follow a curve distinct from the infinite volume solution. It turns out that in both cases this curve can be described by the infinite volume solution multiplied by a constant factor (the dotted lines in the graphs). A similar observation can be made for the second lowest point. As yet we have no full analytical understanding of this observation.

This behaviour has interesting consequences for the running coupling, defined in eq. (2.4) and shown in Figure 4: at least the first two points of every solution on a torus will always remain significantly below the infinite volume solution no matter how large the volume is. Thus on every compact manifold one finds a running coupling which looks infrared suppressed, although the corresponding coupling from the infinite volume limit has an infrared fixed point. Taken at face value this result means that it is extremely difficult if not impossible to verify infrared fixed points of the running coupling in lattice calculations. Indeed, all recent determinations of vertex couplings from lattice QCD find infrared vanishing couplings [36] whereas the infinite volume analysis unambiguously predicts fixed points [24,1,31,32]. Our observation may well serve to explain this discrepancy.

Finally, in the lower panel of Figure 5 we present results for two tori with the same physical volume but different ultraviolet cut-offs given in the legend. The two corresponding solutions for the gluon propagator are close to each other, although one observes a slight distortion of shape from the curve with the small cut-off compared to the one with the larger cut-off and the infinite volume solution. From this result one may conclude that cut-off effects in the DSE-solutions on a torus are small and do not significantly affect the infrared behaviour of the propagators.⁴

3.4 Emergence of the infrared asymptotic behaviour

We now study the rate of approach towards the infinite volume solution in some more detail. Because of the redundancy in the parametrisations (2.20) as discussed in Sec. 2.4, direct fits to our data simultaneously of all free parameters in the these finite-volume infrared forms are not possible. Fits of both screening-mass parameters would in principle be possible from the expressions in Eqs. (2.47). It will turn out, however, that the volumes in our numerical results which range up to approximately $(14 \text{ fm})^4$ are nevertheless still too small for the leading infrared exponent κ_c , or any other momentum and volume independent constant, to describe the data in a reasonable range of momenta. For these volumes the available infrared momenta all lead to values of $1/(k^2 L^2)$ which are beyond the range of validity of the expressions in (2.47), where the exponent κ_c is already close to its infinite volume value but the screening masses $\mu_{Z/G}$ are

⁴ In the light of these results we also conclude that the larger cut-off effects noted in [18] are artefacts of the renormalisation procedure used therein.

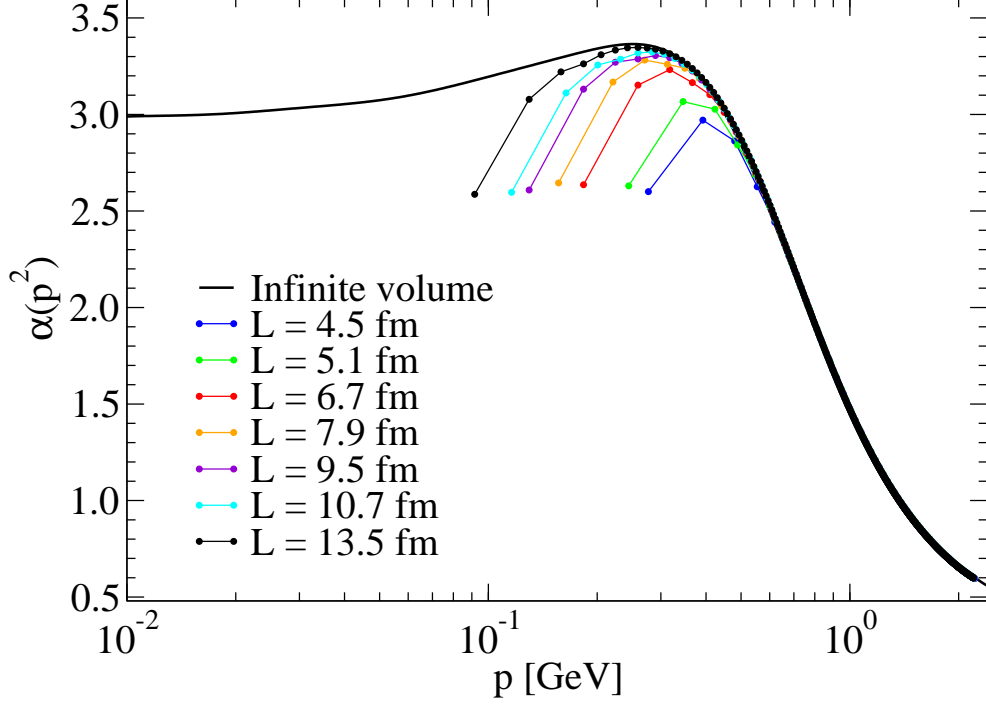


Fig. 4. The running coupling $\alpha(p^2) = \alpha(\mu^2)G^2(p^2)Z(p^2)$ as defined from the ghost-gluon vertex.

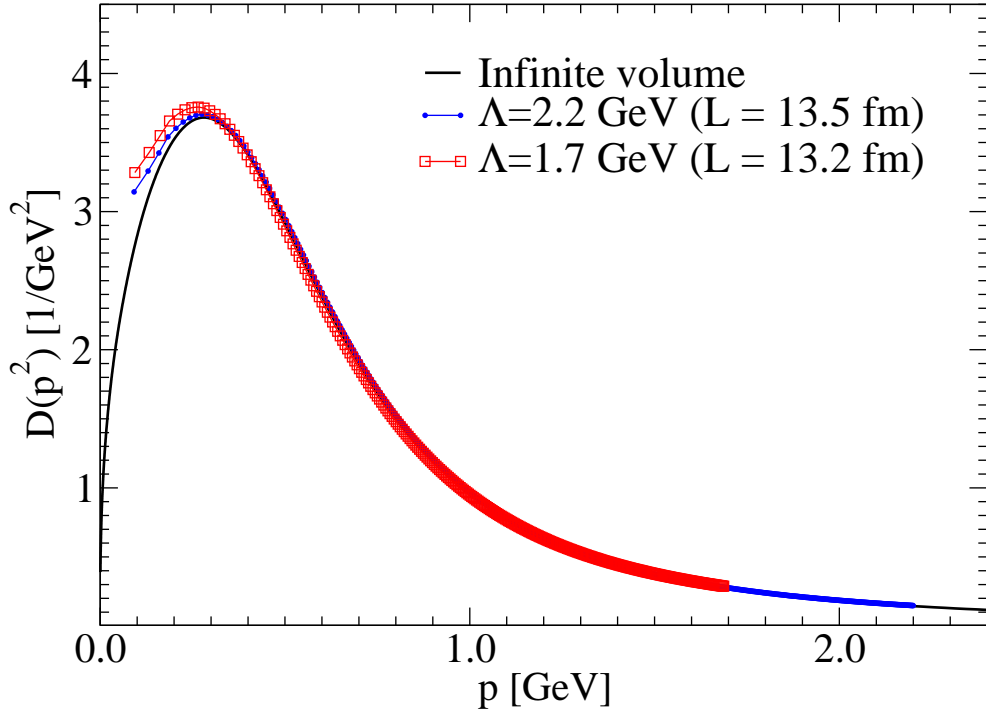


Fig. 5. The gluon propagator calculated on tori with the same physical volume but different ultraviolet cut-offs.

still present. We will find, in fact, that there is not yet a clear separation of scales (1.1) for any momentum in these volumes in the first place.

We therefore adopt two different models, each to fit the data in two steps. To illustrate this procedure we start from the ghost dressing function for which it yields the more stable results in the available volumes than for that of the gluon. Instead of (2.47) we assume a ghost dressing function at low momenta of the form,

$$G_L(k^2) = G_{\text{IR}} \left(\frac{\Lambda_{\text{QCD}}^2}{k^2 + \mu_G^2} \right)^{\kappa_{ghost}}, \quad (3.57)$$

in which we allow both, the screening mass μ_G and the effective exponent κ_{ghost} to depend on the volume, *i.e.*, on L . We then proceed in the following two alternative ways:

- (1) In this model we first set the screening mass to zero, *i.e.*, $\mu_G = 0$ in (3.57), and determine the effective exponent κ_{ghost} by fitting the third to fifth lowest momentum values of the solution for every given volume to the resulting pure power law $\propto (\Lambda_{\text{QCD}}^2/k^2)^{\kappa_{ghost}}$. The results are plotted over the inverse box length as the triangles in the left panel of Fig. 6. We then keep κ_{ghost} fixed and fit in a second step the remaining parameters on a larger region. Here we typically use the lowest eight momenta. The resulting values for ghost screening mass are the triangles in the left panel of Fig. 7 which all lie on a straight line $\propto 1/L$ with offset zero.

The resulting fits are stable with respect to moderate variations of the fit regions in each step (within error bars) and nicely reproduce the same results. Note that this method predominantly absorbs the finite volume effects in the effective exponent. The screening mass essentially accounts only for the remaining mismatch after this first step.

- (2) In this fit-model we adopt the extremely opposite point of view. We first obtain an effective exponent κ_{ghost} which is completely independent of any finite-volume effects by fitting the pure power law form to the infinite volume solution in the same momentum range used in the first step of model (1) above, that of the third to the fifth lowest momentum values of a given torus solution. The resulting values are plotted for comparison as the dots which lie above the triangles, also in the left panel of Fig. 6.

Fitting the remaining parameters to that torus solution then essentially works as in model (1) above. We use the same larger momentum region of the typically eight lowest values, and the fits are similarly stable w.r.t. variations of that region as above. The resulting screening masses are larger than in model (1) and shown as the squares in Fig. 7.

The crucial distinction is that in this second model the finite-volume effects are entirely accounted for by the screening mass alone. For the volumes available the effective exponent κ_{ghost} in (3.57) is not equal to κ_c yet. It changes with the volume because the momentum range where it is obtained does. Nevertheless, this effective exponent is obtained from the infinite volume solution and thus independent of finite volume effects. It rather describes the deviations from the leading infrared behaviour already of the infinite volume solution in the corresponding momentum range, due to the fact that these momenta are not yet far enough below Λ_{QCD} . The volumes are too small to fit a range of momenta (1.1) in.

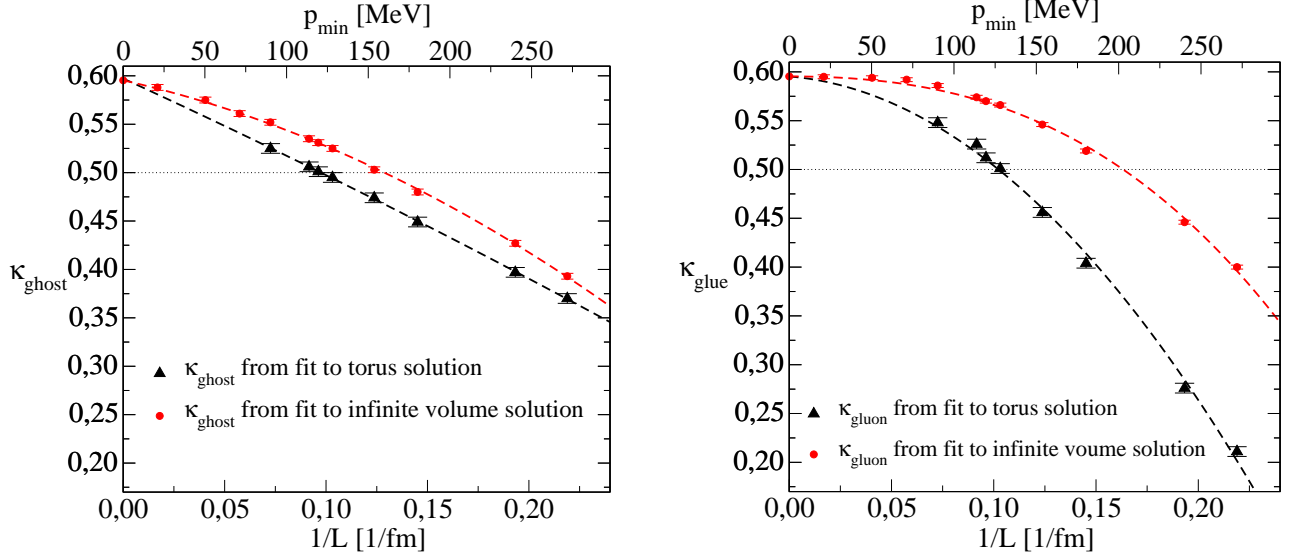


Fig. 6. The infrared exponents κ_{ghost} and κ_{glue} from fits to the torus solutions on different volumes, *c.f.*, model (1) as described in the text, compared to the effective power law fits to the infinite volume solution in the same momentum region for model (2).

The fact that both alternative fit-models are possible reflects the redundancy in our finite-volume infrared parametrisations as mentioned above. In volumes which are not quite large enough for the leading volume asymptotics we can neither describe the data with constant exponent nor without screening mass. Both, an effective exponent and a screening mass are necessary in these volumes. However, to allow this both underconstrains the fits. The two extreme models to fit the data by absorbing a maximum of finite-volume effects either in the effective exponent or the screening mass serve as a measure of this redundancy.

The results approach each other and this redundancy decreases with increasing volumes as expected. In the volumes of the order of up to approximately $(14 \text{ fm})^4$ presented here the mismatch between both models does not quite vanish yet. We can extrapolate the data from both fit-models to larger volumes, however, to make a rough prediction about what volumes are necessary for the unique leading finite-volume infrared behaviour as parametrised in (2.47) to set in. The result gives the following quite consistent overall picture:

Comparing Figs. 6 and 7 we observe that for box lengths of approximately $L = 40 \text{ fm}$ (*i.e.*, $1/L \approx 0.025 \text{ fm}^{-1}$) the effective exponents from torus and infinite volume solutions approach each other and eventually meet extremely close to the asymptotic infinite-volume value $\kappa_c \approx 0.595$. For lengths above 40 fm we therefore expect $\kappa_{ghost} = \kappa_c$ to be a very good approximation. The screening masses are not zero yet, but also approach each other very well at volumes of this size. This means that from our extrapolations we would estimate that the asymptotic forms (2.47) can be expected to describe the finite volume infrared behaviour well for volumes of $L = 40 \text{ fm}$ in size and more.

As described in the previous section, the dressing function of the gluon propagator is more difficult to describe by such fits in the intermediate volumes here because its momentum dependence deviates much more strongly from its infinite-volume infrared asymptotics even at

the lowest momenta available in our volumes. For the gluon dressing function model (1) only leads to stable results for the screening mass μ_Z in our largest volume $V = (13.8 \text{ fm})^4$ which is included in the right panel of Fig. 7. The volume dependence of the gluon dressing function is stronger than that of the ghost. This is apparent from the right panel in Fig. 6 for model (1), with the volume dependence predominantly accounted for by the effective exponent which is obtained from the $\mu_Z = 0$ fits of the form,

$$Z_L(k^2) = Z_{\text{IR}} \left(\frac{k^2}{\Lambda_{\text{QCD}}^2} \right)^{2\kappa_{\text{glue}}}, \quad (3.58)$$

and which depends more strongly on $1/L$ than it does for the ghost. But it again approaches the effective exponent of the infinite volume solution at box lengths of about 40 fm.

In model (2), with no finite-volume effects in the effective exponents, we observe the same stronger volume dependence in the gluonic screening mass μ_Z as compared to μ_G in Fig. 7. Again, however, within the considerable errors,⁵ the extrapolations of the data for the gluonic screening masses from models (1) and (2) are consistent with an approach of the two at about the same length scale of $L = 40$ fm.

Note that the screening-masses of model (1) are extrapolated using linear fits (of the fits) inversely proportional to the length,

$$\mu_{Z/G} \propto 1/L. \quad (3.59)$$

In model (2) on the other hand, our extrapolations of the screening masses are exponential in nature from fits of the form

$$\mu_{Z/G} \propto m (\exp\{l/L\} - 1), \quad (3.60)$$

with dimensionful constants m (in MeV) and l (in fm). In our intermediate volumes both forms differ considerably. At sufficiently large L (with our estimate ≥ 40 fm), however, they both agree with the scaling Ansatz (2.44) used the infrared analysis of Sec. 2.4.

As a final cross-check, for the ratio of the screening masses,

$$\mu_Z/\mu_G \approx \sqrt{238/86} \approx 1.7, \quad (3.61)$$

as obtained from Eqs. (2.46) in Sec. 2.4 for asymptotically large volumes, here we roughly obtain $\mu_Z/\mu_G \approx 1.6$ for their ratio from the corresponding ratio of the slope of the linear fits in model (1), the solid lines through the triangles in Fig. 7. This is in perfect agreement with the

⁵ For the gluonic screening-mass in model (1) we simply draw a straight line between our only value at $L = 13.8$ fm and zero at $1/L = 0$ in Fig. 7 (right).

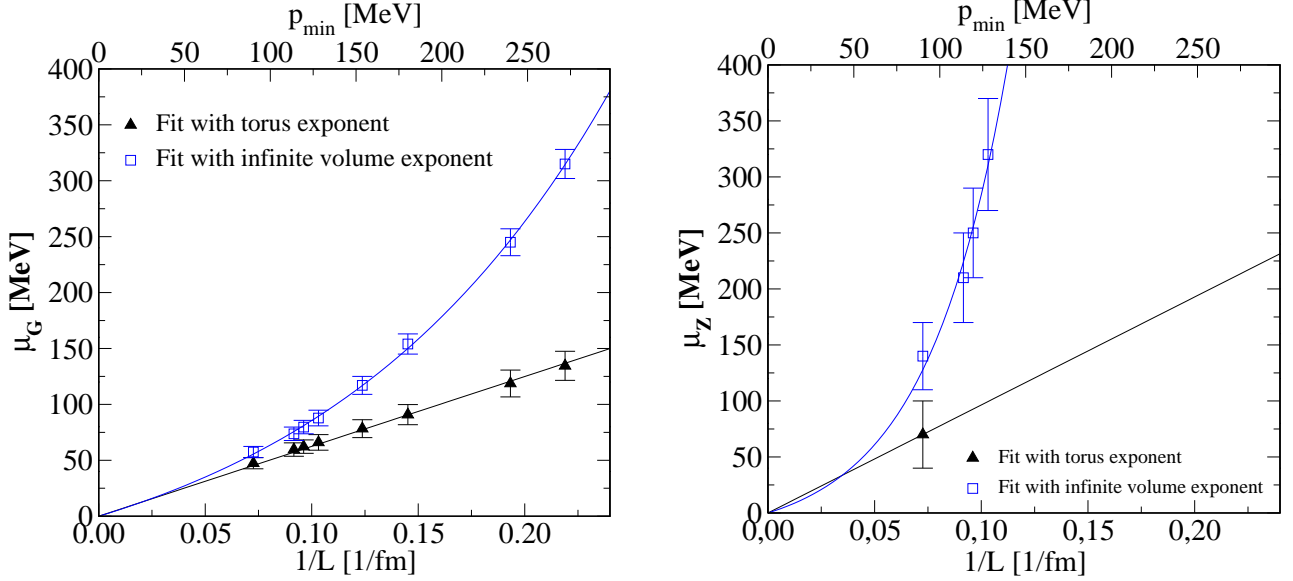


Fig. 7. In the left panel the behaviour of the ghost mass μ_G with the inverse box length $1/L$ is shown. The error of five percent reflects the systematic uncertainty of our fit procedure. The straight line is a linear fit with zero offset. In the right panel the same is shown for the gluon mass μ_Z . However, the systematic uncertainty is larger, about forty percent, see text.

predicted asymptotic ratio (3.61), but the procedure has a large error of around 50%, mainly from the single value $\mu_Z = 70(30)$ MeV in for the $(13.8 \text{ fm})^4$ volume which determines the slope in the gluonic screening mass in model (1).

For the effective exponents of both dressing functions we always use extrapolations (the long dashed lines model (1) and the short dashed for model (2) from the infinite volume solutions) based on quadratic polynomials⁶ in $1/L$ with the $1/L = 0$ value fixed at $\kappa_c \approx 0.595$,

$$\kappa_{fit}(1/L) = \kappa_c - \frac{a_1}{L} - \frac{a_2}{L^2}. \quad (3.62)$$

For the dressing functions in model (1) we have also included the constant term $\kappa_{fit}(0)$ in the quadratic fit of the form (3.62):

From the ghost dressing function this yields $\kappa_{fit}(0) = 0.597(3)$ in perfect agreement with the analytic result of $\kappa_c = 0.595$ at 3-digit precision.

Note that for the gluon dressing function, the model (1) fits using the form (3.62) with fixed κ_c produce a coefficient a_1 of the linear term consistent with zero. Including the constant term in the complete 3 parameter fit is then not stable anymore. It requires dropping the linear term, *i.e.* freezing $a_1 = 0$. Doing so, however, one then obtains $\kappa_{fit}(0) = 0.60(2)$ which is also consistent with the analytic result.

⁶ The only exception here is the effective exponent of the infinite-volume gluon solution, the short dashed line in the right panel of Fig. 6, which requires the inclusion of a cubic term.

Finite volume corrections to κ_c of the form (2.43) used for our infrared analysis in Sec. 2.4 can not reasonably be extracted from our present data. This is not unexpected because it requires volumes of a size at which the scaling relation (2.29), *i.e.*, $\kappa_{Z_L} + 2\kappa_{G_L} = 0$, for the infrared exponents is already valid. Here, *c.f.*, the definition of the effective exponent for our fits in (3.58), this is when

$$\kappa_{glue} \approx \kappa_{ghost} , \quad (3.63)$$

which according to our estimate again requires $L \approx 40$ fm, *c.f.*, Fig. 6, and is thus still relatively far beyond our numerical data to attempt reasonable fits and extrapolations.

We furthermore note that the length scale where the behaviour of the gluon propagator turns from $\kappa < 0.5$ (infrared diverging) to $\kappa > 0.5$ (infrared vanishing) is of the order of at least $L = 6$ fm for model (2) (from the infinite volume effective exponent) up to $L = 10$ fm for model (1). The exact turning point might also be somewhat truncation dependent.

In summary, we have seen in the previous two sections that the qualitative infrared behaviour of the gluon and ghost propagators of Landau gauge QCD starts to emerge in volumes of estimate sizes between $L = 10$ fm and 15 fm. To reliably extract infrared exponents and other quantitative results about their infrared behaviour, one furthermore needs a certain range of momenta with a clear separation of scales (1.1) which requires much larger volumes. The leading finite-size effects are under good control, and can be described by the simple screening masses $\mu_{Z/G} \propto 1/L$ via Eqs. (2.47), when the effective exponents approach their infinite volume scaling behaviour and are sufficiently close to κ_c . Our extrapolation method predicts that this might require volumes of about 40 fm in size.

3.5 Comparison to lattice results

We now compare our results from DSEs on a torus to the ones from lattice calculations. Lattice studies of the Landau gauge gluon propagator have quite a long history already [37,38,39,40,41]. Nowadays, lattice data for the gluon propagator is available on impressively large lattices. The authors of [10] report on an $SU(2)$ -study on a 52^4 -lattice, whereas in [11] results from an $SU(3)$ calculation on a 56^4 -lattice are discussed with larger lattices on their way.⁷ The physical volumes of both these studies are comparable. The resulting propagators are very similar with small deviations for the first few points in the infrared.⁸ In the upper graph of Figure 8 we display the $SU(3)$ -results together with data on a smaller volume [44] and compare with DSE-results on tori with similar volumes.

The qualitative agreement of the solutions at similar volumes in the infrared is striking.⁹

⁷ For results from simulations using large asymmetric lattices, see [42].

⁸ This independence of the number of colours has also been found in an earlier study [43]. However, there a different gauge, the LaPlacian gauge, has been used.

⁹ Differences in the intermediate momentum regime around 1 GeV are truncation artefacts of the

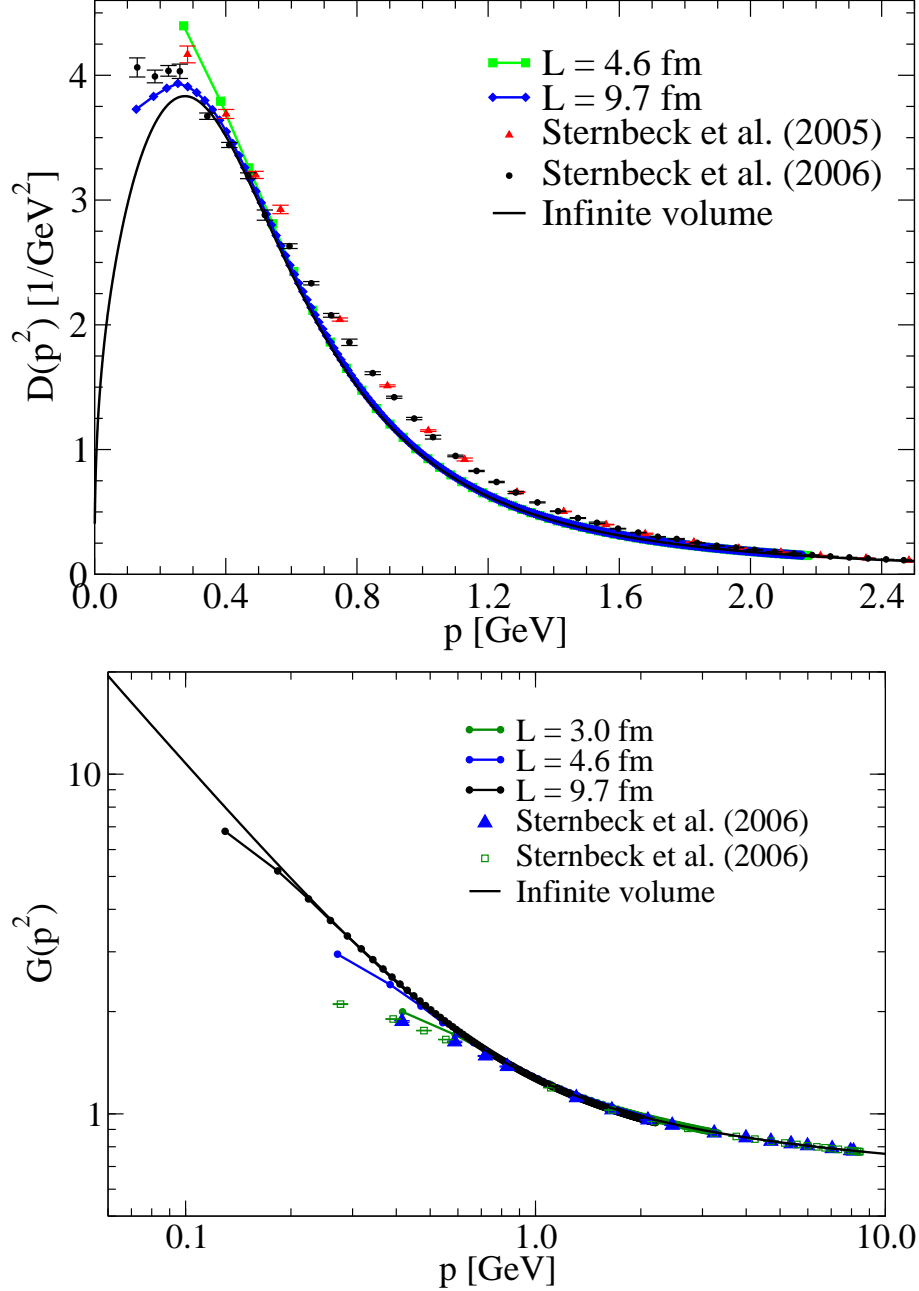


Fig. 8. DSE results for the gluon propagator and ghost dressing function on tori with different volumes compared to recent lattice calculations on similar manifolds. The lattice data are taken from Refs. [11,44].

Whereas both, the lattice and the DSE result at the smaller volume $V \approx (4.6 \text{ fm})^4$ seem to diverge, one starts to observe an infrared finite one, or perhaps even a slight infrared suppression, at the larger volumes $V \approx (9.7 \text{ fm})^4$. This indicates that the scaling behaviour of the lattice results with volume may be very similar to the ones of the DSE solution. If so, then our results

DSE solutions. One can show analytically that this is exactly the region where the omitted gluonic two-loop diagrams contribute significantly.

from the last section predict also a turnover of the lattice data when even larger volumes are considered.

The situation is less clear for the ghost dressing function, which was first studied on the lattice in [45]. Our results for three different volumes, $V = (3.9, 4.6, 9.7 \text{ fm})^4$, are compared to the $SU(3)$ lattice results of [11,44].¹⁰ For the DSE solutions we observe a characteristic deviation of the two lowest momentum points at each volume from the infinite volume solution. As shown in the previous section these deviations correspond to a ghost mass which goes to zero in the infinite volume limit. The lattice results do not seem to show such behaviour as yet. Even though the lattice volumes herein are roughly between 3 fm and 4.5 fm, and thus still rather small compared to our analysis in the previous section, there appears to be not much sign of a volume dependence at all at this point. The situation is indeed reminiscent of the corresponding torus solution from the previous DSE studies. Perhaps revisiting the renormalisation procedure as described in Sec. 3.2 might have a similar influence in the analysis of the lattice data.

In these relatively small volumes, however, some finite-volume effects in our DSE solutions might also still be somewhat truncation dependent and could therefore contribute to the differences between the DSE solutions and on the lattice simulations. Furthermore, effects from Gribov copies are known to influence the lattice results for the ghost propagator much stronger than for the glue. This has been investigated by comparing results from gauge fixing to the first Gribov copy (*fc*) to the results of a more involved procedure of repeated gauge fixing and selecting then the best copy (*bc*). On rather small volumes these two procedures have been compared in [44] and noticeable effects observed. Therefore, a meaningful comparison between the DSE and lattice ghost propagator not only awaits an improved truncation scheme in the DSEs and results on larger volumes on the lattice, but also a further clarification of gauge fixing effects in both, the continuum and lattice studies.

4 Conclusions

The results presented here explicitly demonstrate that Landau gauge propagators from lattice and continuum calculations are compatible, provided finite volume effects are properly taken into account. The approach of the torus solutions towards the infinite volume limit is slow, but steady and quantifiable. Our results show that the characteristic maximum in the gluon propagator should be measurable in volumes of the order $V \approx (10 - 15 \text{ fm})^4$ which come into grasp for lattice calculations. This important qualitative effect will be the hallmark of the onset of the asymptotic infrared region.

The results also demonstrate, however, that extremely large volumes will be necessary for a more quantitative comparison between results in the continuum and on the lattice. The reason is, of course, the requirement (1.1) to observe the asymptotic infrared behaviour. Hence, even

¹⁰ For corresponding results in $SU(2)$ see [46]. To date no systematic lattice study on the effects of the gauge group on the ghost propagator exists.

verifying the scaling of the infrared exponent according to figure 6 requires spanning an enormous range of volumes. Thus the agreement between both methods can be at best qualitative for quite some time to come. That so far not even a very good qualitative agreement could be observed can also be understood with the results presented here. The most characteristic qualitative feature of the gluon propagator is its maximum. To observe it, it is trivially necessary to also observe its infrared suppression. This suppression depends on the quantitative value of the infrared exponent κ_{glue} . In particular, its value in Landau gauge, compared, *e. g.*, to Coulomb gauge, leads to a very weak infrared suppression. Hence very large volumes are necessary to observe this suppression, and hence the maximum.

Nonetheless, if a clear maximum emerges in the gluon propagator on larger lattices, confirming the predictions made here, it will definitely be an important piece in our understanding of the confinement mechanism in Landau gauge.

Finally we would like to remark that all volume effects discussed here are only typical for correlation functions involving intrinsically massless fields. Objects, which have an intrinsic mass-scale, like quarks or hadrons, will only indirectly be affected by such finite volume effects. For quarks these effects may be still significant, as can be seen from the results of [19]. The situation is different, however, for hadrons: the specific far infrared behaviour of the gluon correlation functions are expected to be nearly irrelevant to hadronic observables [1,23,47].

Acknowledgements

We are grateful to Reinhard Alkofer for useful discussions. This work has been supported by the Deutsche Forschungsgemeinschaft (DFG) under contracts Fi 970/7-1, GI 328/1-2, and MA 3935/1-1.

References

- [1] R. Alkofer and L. von Smekal, Phys. Rept. **353** (2001) 281.
- [2] T. Kugo and I. Ojima, Prog. Theor. Phys. Suppl. **66** (1979) 1 [Erratum Prog. Theor. Phys. **71**, 1121 (1984)].
- [3] N. Nakanishi and I. Ojima, “Covariant operator formalism of gauge theories and quantum gravity,” World Sci. Lect. Notes Phys. **27** (1990).
- [4] V. N. Gribov, Nucl. Phys. B **139**, 1 (1978).
- [5] D. Zwanziger, Nucl. Phys. B **412**, 657 (1994).
- [6] T. Kugo, hep-th/9511033.
- [7] R. Sommer, Nucl. Phys. Proc. Suppl. **160** (2006) 27.
- [8] F. D. R. Bonnet, P. O. Bowman, D. B. Leinweber and A. G. Williams, Phys. Rev. D **62** (2000) 051501.

- [9] F. D. R. Bonnet, P. O. Bowman, D. B. Leinweber, A. G. Williams and J. M. Zanotti, Phys. Rev. D **64** (2001) 034501.
- [10] A. Cucchieri and T. Mendes, hep-ph/0605224; and references therein.
- [11] A. Sternbeck, E. M. Ilgenfritz, M. Müller-Preussker, A. Schiller and I. L. Bogolubsky, PoS **LAT2006** (2006) 076.
- [12] A. Cucchieri and D. Zwanziger, Phys. Rev. D **65**, 014001 (2002).
- [13] A. Cucchieri, A. Maas, T. Mendes, in preparation.
- [14] Ch. Lerche and L. von Smekal, Phys. Rev. D **65** (2002) 125006.
- [15] D. Zwanziger, Phys. Rev. D **65** (2002) 094039.
- [16] J. M. Pawłowski, D. F. Litim, S. Nedelko and L. von Smekal, Phys. Rev. Lett. **93** (2004) 152002.
- [17] C. S. Fischer, R. Alkofer and H. Reinhardt, Phys. Rev. **D65** (2002) 094008.
- [18] C. S. Fischer, B. Gruter and R. Alkofer, Annals Phys. **321** (2006) 1918.
- [19] C. S. Fischer and M. R. Pennington, Phys. Rev. D **73** (2006) 034029.
- [20] J. M. Pawłowski, hep-th/0512261.
- [21] A. Cucchieri, T. Mendes and A. R. Taurines, Phys. Rev. D **67** (2003) 091502.
- [22] A. Maas, J. Wambach, B. Grüter and R. Alkofer, Eur. Phys. J. **C37**, No.3 (2004) 335.
- [23] C. S. Fischer, J. Phys. G **32** (2006) R253; and references therein.
- [24] L. von Smekal, R. Alkofer and A. Hauck, Phys. Rev. Lett. **79** (1997) 3591.
- [25] L. von Smekal, A. Hauck and R. Alkofer, Annals Phys. **267** (1998) 1 [Errat. *ibid.* **269** (1998) 182].
- [26] J. C. Taylor, Nucl. Phys. B **33** (1971) 436.
- [27] A. Cucchieri, T. Mendes and A. Mihara, JHEP **0412** (2004) 012.
- [28] A. Sternbeck, E. M. Ilgenfritz, M. Muller-Preussker and A. Schiller, PoS **LAT2005** (2006) 333.
- [29] E. M. Ilgenfritz, M. Muller-Preussker, A. Sternbeck and I. L. Bogolubsky, hep-lat/0609043; A. Sternbeck, PhD Thesis, Humboldt University Berlin, hep-lat/0609016.
- [30] A. Maas, A. Cucchieri and T. Mendes, hep-lat/0610006.
- [31] R. Alkofer, C. S. Fischer and F. J. Llanes-Estrada, Phys. Lett. B **611** (2005) 279.
- [32] C. S. Fischer and J. M. Pawłowski, hep-th/0609009.
- [33] W. Schleifenbaum, A. Maas, J. Wambach and R. Alkofer, Phys. Rev. D **72** (2005) 014017.
- [34] C. S. Fischer and R. Alkofer, Phys. Lett. **B536** (2002) 177.
- [35] C. S. Fischer, PhD thesis, Univeristy of Tübingen, 2003, hep-ph/0304233.

- [36] P. Boucaud, J. P. Leroy, J. Micheli, O. Pene and C. Roiesnel, JHEP **9812** (1998) 004 [hep-ph/9810437]; P. Boucaud, J. P. Leroy, J. Micheli, O. Pene and C. Roiesnel, JHEP **9810** (1998) 017 [hep-ph/9810322]; H. Nakajima and S. Furui, Nucl. Phys. Proc. Suppl. **129** (2004) 730 [hep-lat/0309165]; S. Furui and H. Nakajima, hep-lat/0309166.
- [37] J. E. Mandula and M. Ogilvie, Phys. Lett. B **185** (1987) 127.
- [38] C. W. Bernard, C. Parrinello and A. Soni, Phys. Rev. D **49** (1994) 1585.
- [39] P. Marenzoni, G. Martinelli and N. Stella, Nucl. Phys. B **455** (1995) 339.
- [40] H. Aiso, M. Fukuda, T. Iwamiya, A. Nakamura, T. Nakamura and M. Yoshida, Prog. Theor. Phys. Suppl. **122** (1996) 123; H. Aiso, J. Fromm, M. Fukuda, T. Iwamiya, A. Nakamura, M. Stingl and M. Yoshida, Nucl. Phys. Proc. Suppl. **53** (1997) 570.
- [41] D. B. Leinweber, J. I. Skullerud, A. G. Williams and C. Parrinello, Phys. Rev. **D58** (1998) 031501; *ibid.* **D60** (1999) 094507.
- [42] P. J. Silva and O. Oliveira, Nucl. Phys. B **690** (2004) 177; Phys. Rev. D **74** (2006) 034513.
- [43] C. Alexandrou, P. De Forcrand and E. Follana, Phys. Rev. D **65** (2002) 117502.
- [44] A. Sternbeck, E. M. Ilgenfritz, M. Mueller-Preussker and A. Schiller, Phys. Rev. D **72** (2005) 014507.
- [45] H. Suman and K. Schilling, Phys. Lett. B **373** (1996) 314.
- [46] J. Gattnar, K. Langfeld and H. Reinhardt, Phys. Rev. Lett. **93** (2004) 061601; J. C. R. Bloch, A. Cucchieri, K. Langfeld and T. Mendes, Nucl. Phys. B **687** (2004) 76.
- [47] A. Höll, C. D. Roberts and S. V. Wright, nucl-th/0601071.